

# Radioactivity distributions and biohazard assessment of coastal marine environments of niger-delta, Nigeria

Maxwell Omeje, Muyiwa M. Orosun, Godfrey U. Aimua, Olusegun O. Adewoyin, Soheil Sabri, Hitler Louis, Emmanuel S. Joel, Conrad A. Omohinmin, Eze F. Ahuekwe, Patrick O. Isibor, Mojisola R. Usikalu, Ifeanyi A. Oha, Nuradeen N. Garba & Terkaa V. Targema

To cite this article: Maxwell Omeje, Muyiwa M. Orosun, Godfrey U. Aimua, Olusegun O. Adewoyin, Soheil Sabri, Hitler Louis, Emmanuel S. Joel, Conrad A. Omohinmin, Eze F. Ahuekwe, Patrick O. Isibor, Mojisola R. Usikalu, Ifeanyi A. Oha, Nuradeen N. Garba & Terkaa V. Targema (2024) Radioactivity distributions and biohazard assessment of coastal marine environments of niger-delta, Nigeria, All Earth, 36:1, 1-19, DOI: [10.1080/27669645.2023.2299109](https://doi.org/10.1080/27669645.2023.2299109)

To link to this article: <https://doi.org/10.1080/27669645.2023.2299109>



© 2023 The Author(s). Published by Informa UK Limited, trading as Taylor & Francis Group.



Published online: 29 Dec 2023.



Submit your article to this journal [↗](#)



Article views: 578



View related articles [↗](#)



View Crossmark data [↗](#)

## Radioactivity distributions and biohazard assessment of coastal marine environments of niger-delta, Nigeria

Maxwell Omeje<sup>a</sup>, Muiyiwa M. Orosun<sup>b,c</sup>, Godfrey U. Aimua<sup>a</sup>, Olusegun O. Adewoyin<sup>a</sup>, Soheil Sabri<sup>d</sup>, Hitler Louis<sup>e,f</sup>, Emmanuel S. Joel<sup>g</sup>, Conrad A. Omohinmin<sup>h</sup>, Eze F. Ahuekwe<sup>h</sup>, Patrick O. Isibor<sup>h</sup>, Mojisola R. Usikalua<sup>a</sup>, Ifeanyi A. Oha<sup>i</sup>, Nuradeen N. Garba<sup>j</sup> and Terkaa V. Targema<sup>k</sup>

<sup>a</sup>Department of Physics, College of Science and Technology, Covenant University, Ota, Nigeria; <sup>b</sup>Department of Interdisciplinary Studies, University of Religions and Denominations, Qom, Iran; <sup>c</sup>Department of Physics, University of Ilorin, Ilorin, Nigeria; <sup>d</sup>Durban Digital Twin Lab. School of Modelling, Simulation, and Training, University of Central Florida, Florida, USA; <sup>e</sup>Department of Research Analytics, Saveetha Dental College and Hospitals Saveetha Institute of Medical and Technical Sciences Saveetha University, Chennai, India; <sup>f</sup>Department of Chemistry, University of Calabar, Calabar, Nigeria; <sup>g</sup>Department of Earth Sciences, Anchor University, Lagos, Nigeria; <sup>h</sup>Department of Biological Sciences, College of Science and Technology, Covenant University, Ota, Nigeria; <sup>i</sup>Department of Geology, University of Nigeria, Nsukka, Nigeria; <sup>j</sup>Department of Physics, Faculty of Science, Ahmadu Bello University, Zaria, Nigeria; <sup>k</sup>Department of Physics, Taraba State University, Jalingo, Nigeria

### ABSTRACT

The Unumherin community in Nigeria's Niger Delta is home to coastal marine polluted zones, and this research examines the radioactivity distributions and biohazard in the coastal environment. The activity concentrations of  $^{40}\text{K}$ ,  $^{238}\text{U}$ ,  $^{232}\text{Th}$ , as well as the outdoor dose rate of contaminated coastlines were measured using a calibrated RS-125 Gamma-Spec and a NaI(Tl) gamma-detector. The laboratory examination of sediments, water, and fish from the same coastal region – *Clarias gariepinus*, *Pseudotropheus elongatus*, *Oreochromis niloticus* and *Stromateus fiatola* – was combined with the in-situ observations of gamma dose rates. With a value of  $100\text{nGy/h}$ , the hotspot at site 4 is shown by the geographic distribution of gamma dose rates. The findings showed that the activities of the primordial radionuclides varied, with average values for the sediments and water exceeding suggested limits. Similarly, the corresponding mean hazard indices mostly exceeds the allowable limits. The species specificity of the fish species accounts for the variation in the mean concentrations of  $^{40}\text{K}$ ,  $^{238}\text{U}$  and  $^{232}\text{Th}$ . *C. gariepinus*, having accumulated higher concentrations of  $^{40}\text{K}$  and  $^{238}\text{U}$ , may be the first to elicit health hazards in the future if pollution continues unmonitored. Hence, continuous monitoring of the aquatic environment alongside is highly recommended.

### ARTICLE HISTORY

Received 28 April 2023  
Accepted 12 December 2023

### KEYWORDS



Radioactivity; microbial interaction; bioaccumulation; pollution; niger delta

## 1. Introduction

Naturally occurring radionuclides (NOR) can be transferred from soil to animals and ultimately to humans (Isinkaye & Emelue, 2015). In animals, radionuclides may come as poisonous elements and induce bioaccumulation and bioconcentration, thereby bringing hostile consequences to human and their entire environment. Therefore, assessment of radionuclide concentration in sediments and soils plays a vital role in strategizing appropriately from those disastrous effects of background exposure (Sattar, 2021; Uluturhan et al., 2011).

The amount of radioactivity in the coastal areas could have their source from some natural elements present in the Earth's crust which exist in the terrestrial ecosystem or from human-caused sources (Liu et al., 2008; Uluturhan et al., 2011). Radioactivity measurement is an indicator of hazard to the aquatic habitat from man-made sources like industrial and mining activities (Garba et al., 2016). Nyarko et al. (2011) and

Omeje et al. (2020) suggest that the lack of vital information and awareness in the West African coastal region, can be attributable to the rising radioactivity levels in the face of nuclear activities, agricultural production, industrialisation, mining, offshore gas, and oil exploration. The human exposure to background ionising radiation may emanate from primordial radionuclides of terrestrial origin (Ajibola et al., 2022; Orosun et al., 2021, 2022). These radiations from the primordial radionuclides ( $^{234}\text{Th}$ ,  $^{238}\text{U}$  and their progenies) that emanate from the sediments, internally affects human respiratory tracks (Isinkaye & Emelue, 2015). Understanding the toxicodynamics of radionuclides in natural ecosystems may enhance knowledge on the health implications over an extended period. These NOR enter the tissues of marine fauna via ingestion or absorption and hence are incorporated into the food chain and ultimately pose threats to humans upon ingestion of marine foods (Abbasi & Mirekhtiari, 2020). Therefore, a measurement of the

**CONTACT** Muiyiwa M. Orosun  [muyiwaorosun@yahoo.com](mailto:muyiwaorosun@yahoo.com)  Department of Interdisciplinary Studies, University of Religions and Denominations, Qom, Iran

© 2023 The Author(s). Published by Informa UK Limited, trading as Taylor & Francis Group.

This is an Open Access article distributed under the terms of the Creative Commons Attribution-NonCommercial License (<http://creativecommons.org/licenses/by-nc/4.0/>), which permits unrestricted non-commercial use, distribution, and reproduction in any medium, provided the original work is properly cited. The terms on which this article has been published allow the posting of the Accepted Manuscript in a repository by the author(s) or with their consent.

existing radioactivity with its corresponding radiological hazard is vital to improve and sustain the aquatic environment (Abbasi & Mirekhtari, 2020).

Studies on marine life and human health have been widely explored over the years due to various forms of persistence, bioaccumulation and toxic pollutants sourced from downstream anthropogenic activities that traverse the food chain (Gan et al., 2017). Wang et al. (2018) and Yin et al. (2023) highlighted the predisposition of some aquatic microbes to various types of contamination, and how this may affect their vital roles in the energy flow and material cycling of ecosystems. Microbiological assessment offers low cost, rapidity, simultaneous reflection, simplicity, and low sample consumption for diagnosing soil pollution, assessing the status of other pollutants and elements (Bullo & Bayisa, 2022; Tang et al., 2019; Tang et al., 2022). Biological indicators can be made from microorganisms that are highly sensitive to any kind of pollution (Savvaidis et al., 2001). Its functions in the microbial community can be suitably used as indicators that will reflect pollution, and by considering the microbial diversity and structure of the comprehensive community, at the moment, not much research has been done on using any microbial function to diagnose soil quality (Tang et al., 2019).

Furthermore, researchers have decided to approach the interpretation and quantification of ocean sediment and seafood quality parameters and their attendant risks to humans and the ecosystem in an environment (Singh et al., 2018). Moreover, industrialisation and urbanisation in developing countries may have negative impacts in contaminating ocean and river (Dong et al., 2022; Othman et al., 2012). Ocean and river water management enhances ecological services, reduces environmental problems and improves the water resources that humans rely on (Sakthivadivel et al., 2020; Wu et al., 2019; Yin et al., 2023). Assessing ocean or river is essential to the evaluation of health risk inclination or declination. To sustain and improve the health status of the ocean, adequate assessment of the ecological situation is needed as a compliance indicator and diagnostic indicator (Singh et al., 2018; Yin et al., 2023).

The populace of Niger Delta has been deprived of its traditional means of livelihood such as fishing and other water resources by the unfortunate oil pollution of the marine environment. This situation has been the reason behind a sophisticated trend of communal crisis and deaths since late 1990s (Abosede, 2020). The vast destruction of marine and land resources has been mostly caused by oil corporations' human activities, including gas flaring and oil spills. The region experienced more acid rain as a result of the release of high amounts of sulphur and nitrogen oxides into the Niger Delta ecosystem (Zhao et al., 2023). When ultraviolet light is present, most combustion processes cause the

release of nitrogen and a decrease in the proportion of hydrocarbons, which leads to smog. The impact played a part in the local air and water pollution (Abdulwahid, 2023; Bouazza et al., 2022; Osuagwu et al., 2018; Sudhakar et al., 2022). The level of pollution in the Niger Delta may be among the worst in the world compared to other delta regions of a similar size (Osuagwu et al., 2018). Scientists and environmentalists have estimated the varying magnitude and frequency of oil spills in the region (Abosede, 2020). Furthermore, risk assessment has been shown to be a useful scientific tool that helps policymakers and law enforcement handle contaminated sites in the most economical way possible while protecting the environment and public health (Nazir et al., 2015).

This study aimed to evaluate the radiological and bioaccumulation exposure that may have led to the death of fish and its potential risks to the inhabitants of the Unumherin community in the Niger Delta.

## 2. Geographical and geological information of the study area

The Niger Delta Basin, located southwest of the Benue Trough, connects the Gulf of Guinea and the Niger Delta. It's near Nigeria's western coast and has access to Equatorial Guinea, Cameroon, São Tomé, and Príncipe. (Tuttle et al., 199). The hydrocarbon system found in the complex and very valuable basin is rich and productive. Among Africa's greatest subaerial basins is this one. The sediment fill is formed of many geologic strata and varies in depth from 9 to 12 km, suggesting the potential of basin formation.

Two settlements in the Warri area of the Niger Delta were selected for this research from Unumherin settlements in Delta State in Nigeria, situated between latitudes 4.264825o– 5.414860o North of the Equator and longitudes 5.372116o–6.727176o East of Greenwich (Adegoke et al., 2017).

The Niger Delta region's geology encompasses over 256,000km<sup>2</sup>. The earlier, transgressive Paleocene pro-delta which was formed as a delta and developed in discrete mini basins was the first to be constructed (Adegoke et al., 2017; Tuttle et al., 1999). The tectonic configuration of these micro basins varies, encompassing extensional, translational, and compressional toe – thrust zones. The Ameki Group and Imo Formation comprise outcropping units in the Niger Delta, with subsurface units comprising continental Benin Sands, Agbada formation, and Akata shales (d'Almeida et al., 2016; Adegoke et al., 2017). Oil and gas reserves are estimated to be 40 billion barrels and 40 trillion cubic feet, respectively (Adegoke et al., 2017). Figure 1 depicts the study area's location and geology.

The delta sequence comprises a regressive association of Tertiary clastic rocks up to 12 km thick,

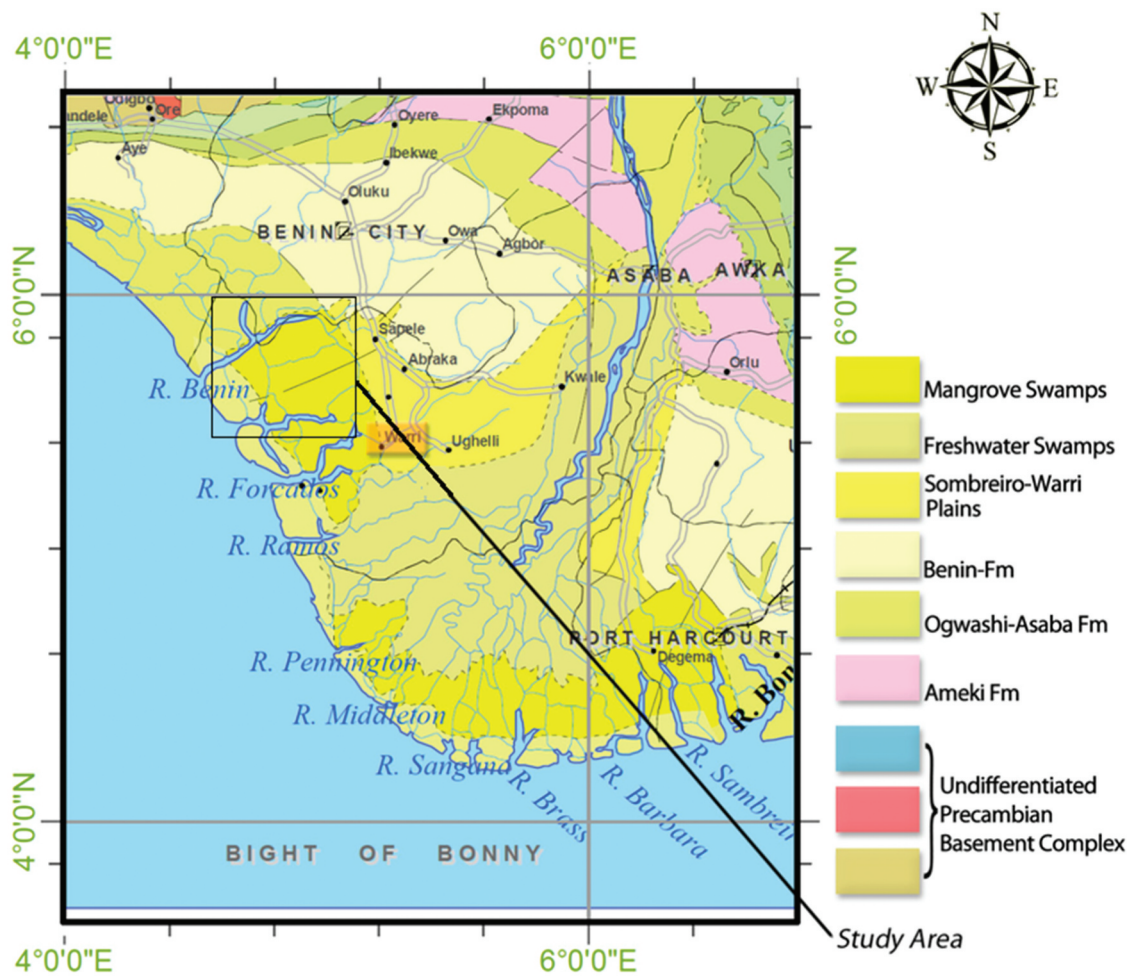


**Figure 1.** Niger delta map showing the study area (modified after (Akpoborie et al., 2015)).

separated into three major lithofacies: claystone, marine shale, siltstone, clay stone, and sandstone. Delta structure and stratigraphy are closely related, with post- and sync-sedimentary lithic normal faults impacting development (d'Almeida et al., 2016; Adegoke et al., 2017).

### **2.1. The unumerhin community's atlantic coastline sediments and the ethiope river**

The Unumerhin Community and Ethiope's Atlantic Coast features natural features providing access to the Atlantic Ocean and Ethiope River for domestic water consumption and fishing (Omeje et al., 2020). The Atlantic coastal sediments of Escravos, Forcados, Burutu, and Agbarho, near the Ethiope River and Umherin Community, contain mudflats, salt marshes, and inner sandy flats. The sediments contain high levels of iron, phosphate, nitrate, and sulphates (Mutiu et al., 2013). The intertidal zone is reached when the capacity of the tidal water along the river and ocean declines, increasing sediment deposition and reducing grain size. The secondary agents brought about by waves that reorganise the

sediments in the research area appear to alter these processes.

## **3. Method of sample collection and preparation**

### **3.1. Measurements of in situ gamma spectroscopy with a super-spec RS125 gamma spectrometer**

Around one metre above the ground, in situ measurements of the background gamma dose rates and the activity concentrations of  $^{40}\text{K}$ ,  $^{232}\text{Th}$ , and  $^{238}\text{U}$  were conducted using a Super SPEC RS-125 gamma detector coated with a 2.0 cm  $\times$  2.0 cm NaI crystal. In order to estimate the variation in the radionuclides within the study area and to accurately measure the radioactivity levels in the sediment samples, the background gamma dose level in the study area was measured in the middle of the dry season using a portable radiation detector (Super – SPEC RS – 125) from Canadian Geophysical Inc (Omeje et al., 2020). The device is ideal for detecting radionuclides and measuring dosage exposure, offering high precision with a  $\pm 5\%$  measurement error (Joel et al.,

2021; Omeje et al., 2020; Orosun et al., 2020, 2020). The integrated design, direct assay read-out values, weather-resistant data point storage, high sensitivity, and ease of use characterise portable equipment. The count shows on the front side of the panel for the RS-125 Super-SPEC at a 1/sec update rate, measured in cps. The RS-125 Super SPEC's variable rate counts SCAN mode typically uses Bluetooth to connect to the hand-held device's external storage to record data in the memory of the device (Omeje et al., 2021). By using the device's Bluetooth connection to connect the external global positioning system (GPS) to the data stream, the locations were found. In the research region, measurements were taken every 20 m, going from places where there was a lot of soil sediment deposition to places where there was less sediment deposition and worn surface areas. A small number of reduced sedimentation zones from riverbanks and the coastline were used as controls. Two measurements were made at each station, and the average of those measurements served as the site's actual data point (Omeje et al., 2020). A sand sample was taken at each measurement location in order to count the particles using gamma-ray spectroscopy in a lab. The RS-125 Super SPEC assay mode provides natural background gamma dose measurements, and dose rate data are directly obtained in  $nGy/h$  (Adagunodo et al., 2018; Omeje et al., 2018, 2021; Orosun et al., 2019). The RS-125 Super SPEC includes utility software for downloading statistics records, while ArcGIS (version 10.8) was used for spatial analysis, processing, georeferencing, and interpolation of measured data.

#### 4. Sampling

Sixteen (16) soil samples, water, and five fish species were collected from the Warri Area of the Niger Delta, following International Atomic Energy Agency (IAEA) (1989) instructions for soil samples collection. For microbiological analysis, separate aseptic samples of water and sediment were collected in sterile containers (Wang et al., 2019). Between February 8 and 14 February 2021, all samples were collected from the designated sites of the Unumherin Community; Figure 2 illustrates these locations. The packing was done using black polythene bags that were taped up and labelled with the location, a pre-established site code, and the sample coordinates. There was a minimum of 20 m between each sampling point. The samples were taken at depths of 10 to 50 cm (vertical distance) using a hand trowel. In the sediments area of the Unumherin community, 15 separate samples of soil sediments were collected at each station of the recorded gamma rays, together with the in-situ background gamma readings at each location. A control sample was obtained from outside the study territory. The samples were analysed at Covenant University's Microbiology Laboratory, where they were removed of impurities and air dried for three days. The samples were then reduced in size and dried again for 24 h to achieve a consistent weight. Water samples were collected in high-density polyethylene containers, rinsed twice with distilled and ultrapure water, and cleaned in 10% nitric acid solution. Airtight polyethylene bags were used, and 5 ml of nitric acid was added to each litre.

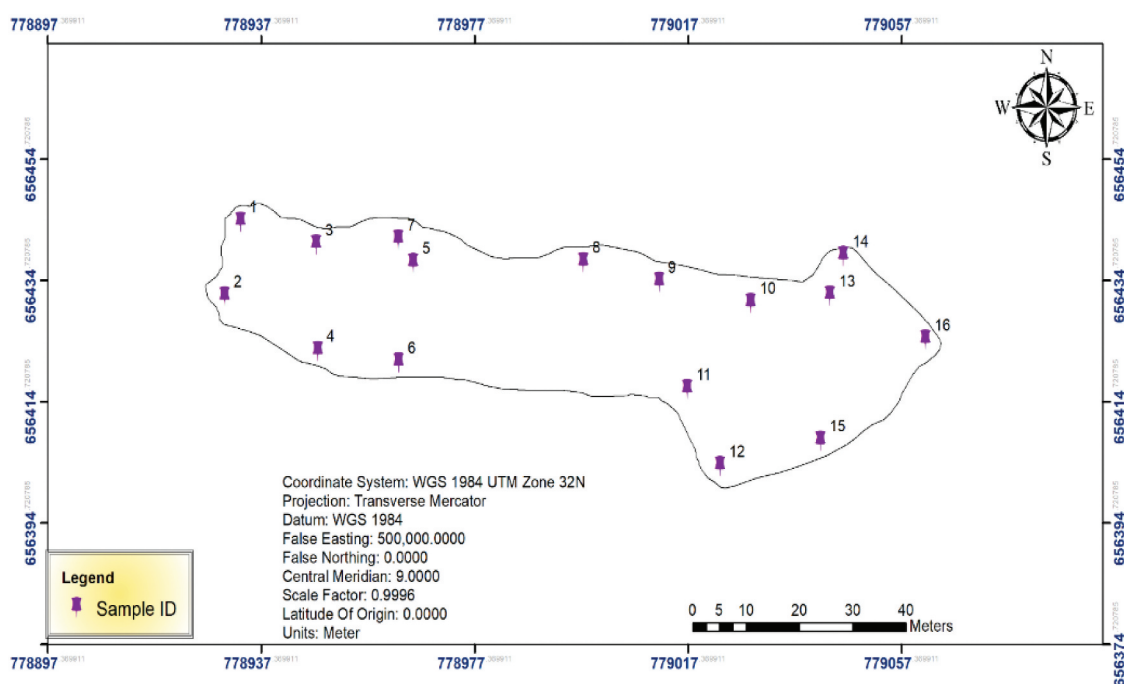


Figure 2. Sample collection points on the base map of the study area.

#### 4.1. Sample preparation and detector calibration for analysis using gamma spectroscopy

Sediment samples were collected, labelled, and shipped to Ahmadu Bello University's Centre for Energy Research and Training in Zaria, Nigeria, where they were dried until mass remained unaltered. The desiccated specimens were meticulously crushed, broken down, and ground into a fine powder. A 2 mm sieve was used to filter the powder. Of the samples (dry weight), only 200 g to 300 g were used for analysis due to the detector shield's limited capacity. Cases were triple-sealed with Vaseline jelly, candle wax, and adhesive masking tape to prevent  $^{222}\text{Rn}$  from escaping, ensuring safe storage and handling.

Upon weighing, the samples were placed within uniformly sized, radon-impermeable, cylindrical plastic containers (70 mm in height by 60 mm in diameter), which were sealed and kept that way for about 30 days (Jibiri et al., 2009). This was done so that, before gamma spectroscopy, radon and its short-lived offspring might achieve secular radioactive equilibrium. Additionally, the reference material was moved to a container with the same specifications as the ones used for the sediment sample collection. For the radioactivity measurements, a lead-shielded 76 × 76 mm NaI(Tl) detector crystal (Model No. 727 series, Canberra Inc.) was utilised, connected through a preamplifier to a Canberra Series 10 plus multichannel analyser (MCA) (Model No. 1104) (Niese, 197). At an energy of 662.0 KeV ( $^{137}\text{Cs}$ ), its resolution (FWHM) of roughly 8% is deemed sufficient to differentiate the gamma-ray energies of interest in the current investigation. Given the limited energy resolution of the NaI(Tl) detector employed in this investigation, consideration was given to the selection of gamma-ray peaks of the radionuclides to be used for measurements. The study ensured proper distinction of photons released by radionuclides by determining their energy and emission probability, and minimising background continuum. The daughter radionuclide  $^{208}\text{Tl}$  indicated  $^{228}\text{Th}$  and  $^{214}\text{Bi}$   $^{226}\text{Ra}$ , while the 1460 KeV  $\gamma$ -rays released during potassium-40 disintegration were measured.

Fish samples were arranged on a detector, monitored for 29,000 s, and the net area beneath peaks in the energy spectrum was calculated by deducting counts from peaks.

**Table 1.** Windows of spectral energy utilised in the analysis.

NOR	Energy (KeV)	Window (KeV)
Th – 232	2614.5	2480 – 2820
R – 226	1764.0	1620 – 1820
K – 40	1460.0	1380 – 1550

#### 4.2. Energy calibration

The system was calibrated using  $^{137}\text{Cs}$  and  $^{60}\text{Co}$  calibration point sources, providing 72% energy resolution for the 661.7 keV of Cs-137, and analysed using the spectral energy windows listed in Table 1.

#### 4.3. Radiological hazard indices estimation

##### 4.3.1. Absorbed dose rate

Equations 1 and 2 were used to estimate the airborne absorbed dose rates ( $D_{outdoor}$  and  $D_{indoor}$ ) caused by the specific activities of  $^{40}\text{K}$ ,  $^{238}\text{U}$ , and  $^{232}\text{Th}$  ( $\text{Bqkg}^{-1}$ ) in samples of contaminated coastlines (UNSCEAR, 2000).

$$D_{outdoor} (\text{nGyh}^{-1}) = 0.462C_u + 0.604C_{Th} + 0.041C_K$$

$$D_{indoor} (\text{nGyh}^{-1}) = 0.92C_u + 1.1C_{Th} + 0.08C_K$$

where  $C_K$ ,  $C_U$ , and  $C_{Th}$  are the activities of  $^{40}\text{K}$ ,  $^{226}\text{Ra}$ , and  $^{232}\text{Th}$  respectively in the sampled tiles.

##### 4.3.2. Annual effective dose for external exposures ( $AED_{Ext}$ )

The dose rates provided in the expressions below were utilised to determine the annual effective dosage for external exposure that individuals would receive.

$$AED_{outdoor} (\mu\text{Svy}^{-1}) = D_{outdoor} (\text{nGyh}^{-1}) \times 8760h \times 0.7 (\text{SvGy}^{-1}) \times 0.2 \times 10^{-3}$$

$$AED_{indoor} (\text{mSvy}^{-1}) = D_{indoor} (\text{nGyh}^{-1}) \times 8760h \times 0.7 (\text{SvGy}^{-1}) \times 0.8 \times 10^{-6}$$

An indoor occupancy factor of 0.8 and a dose conversion factor of  $0.7\text{SvGy}^{-1}$  were chosen (UNSCEAR, 2000).

##### 4.3.3. Annual effective dose for ingested radionuclide ( $AED_{Ing}$ )

The yearly effective dose rate for each radionuclide ingested through food (fish) and water was calculated using equation (5).

$$AED_{Ing} = 365 \sum I_i \times D_i$$

Where  $I_i$  is the daily intake of radioactive material ( $\text{Bq d}^{-1}$ ) = (radioactive material concentration in food or water, expressed in  $\text{Bqkg}^{-1}$  or  $\text{Bq l}^{-1}$ ) × (food or water consumption rate, expressed in  $\text{kg d}^{-1}$  or  $\text{l d}^{-1}$ ), and  $D_i$  is the adult dose conversion factor, or ingestion dose coefficient.  $D_i$  is  $6.2 \times 10^{-9}$ ,  $2.3 \times 10^{-7}$  and  $4.5 \times 10^{-8} \text{SvBq}^{-1}$  for  $^{40}\text{K}$ ,  $^{234}\text{Th}$  and  $^{238}\text{U}$ , respectively (International Commission on Radiological Protection ICRP, 2012; UNSCEAR, 2000). The assumption that an adult's daily water intake is  $2 \text{l d}^{-1}$  was used to estimate the annual effective dosage arising from water consumption. Meanwhile, Nigeria's per capita fish consumption is barely 11.2 kg, compared to the 18.7 kg average annual global per person

consumption (VANGUARD, 2014). This means that the daily fish intake per person in Nigeria is  $0.031\text{kgd}^{-1}$ . This information was used to calculate the annual effective dose that comes from consuming fish from the Niger Delta's coastal marine environment.

#### 4.3.4. Radium Equivalent Activity Index ( $Ra_{eq}$ )

The following formula was used to determine the radium equivalent ( $Ra_{eq}$ ):

$$Ra_{eq} = C_{Ra} + 1.43C_{Th} + 0.077C_K$$

where  $C_{Ra}$ ,  $C_{Th}$ , and  $C_K$  are the radioactivity concentrations in  $\text{Bqkg}^{-1}$  of  $^{226}\text{Ra}$ ,  $^{232}\text{Th}$  and  $^{40}\text{K}$ , respectively.

#### 4.3.5. Representative level index (RLI)

The Representative Level Index (RLI) was evaluated using the expression provided by equation 6 (Omeje et al., 2020; UNSCEAR, 2000):

$$RLI = \frac{C_{Ra}}{150} + \frac{C_{Th}}{100} + \frac{C_K}{1500}$$

where  $C_{Ra}$ ,  $C_{Th}$ , and  $C_K$  maintain their usual definition.

An  $AED \leq mSv$  is represented by RLI values = 1. Therefore, in order to screen building materials that contain considerable concentrations of these NOR and evaluate the risk of gamma radiation linked with them, RLI is the suitable radiological impact parameter (UNSCEAR, 2000).

#### 4.3.6. Radiation Hazard Indices

The level of  $\gamma$ -radiation hazard connected to the naturally occurring radionuclide in samples was estimated using these indices. Equations (8) and (9) were used to determine the radiation hazards associated with the external ( $H_{ext}$ ) and internal ( $H_{int}$ ) respectively.

$$H_{ext} = \left(\frac{C_U}{370}\right) + \left(\frac{C_{Th}}{259}\right) + \left(\frac{C_K}{4810}\right)$$

$$H_{int} = \left(\frac{C_U}{185}\right) + \left(\frac{C_{Th}}{259}\right) + \left(\frac{C_K}{4810}\right)$$

For the radiation risk to be insignificant,  $H_{int}$  must be less than unity.

#### 4.3.7. Excess lifetime cancer risk (ELCR)

Equation (10) was used to determine the excess lifetime cancer risk (ELCR):

$$ELCR = AED \times DL \times RF$$

where the average life expectancy (DL) is taken to be 70 years, the annual effective dose (AED), and fatal cancer risk per Sievert (RF) are estimated for a

population with a recommended ELCR of 0.05 (UNSCEAR, 2000).

#### 4.3.7.1. Annual gonadal equivalent dose (AGED)

Using the examined samples, the AGED for the general public was assessed using the subsequent formula (UNSCEAR, 2000):

$$AGED(\mu\text{Svy}^{-1})C = 3.09C_U + 4.18C_{Th} + 0.314C_K \quad 11$$

### 4.4. Isolation and enumeration of microbial population

By homogenising one gram of the sediment sample and one millilitre of the water sample in nine millilitres of sterile physiological saline solution (0.85% NaCl) and serially diluting to  $10^3$ , the number of microbial isolates recovered from the water and sediment samples were determined. For fungal culture, 1 ml of the  $10^3$  dilutions was aseptically plated on molten Sabouraud dextrose agar (SDA) by the pour plate method in triplicate. The media was sterilised at 15 psi for 15 minutes, supplemented with 100 mg/l chloramphenicol to preclude bacterial growth before inoculation, and incubated at 25 °C for 5 to 7 days. Pure cultures were subcultured and identified on the basis of morphologic and microscopic differentiation upon lactophenol cotton blue staining and then stored in SDA slants (Ahmad et al., 2023; Gautam & Bhadauria, 2012; Ire & Ahuekwe, 2016).

Using the pour plate technique, 0.1 ml of each of the  $10^3$  homogenate dilutions were inoculated in triplicate on Petri plates holding 15 ml of molten nutrient (Oxoid, UK) and MacConkey (Oxoid CM 516, UK) agar for bacterial culture. In all cases, for nutrient agar, the media were supplemented with 0.015% (w/v) nystatin to inhibit fungal growth after sterilization at 15 psi for 15 min and incubated at 37 °C for 24 to 48 h (Wang et al., 2019). Discrete colonies were noted and purified by a subculture for further identification via Gram staining, biochemical characterisation, and storage as pure cultures in agar slants. Following standard methods, biochemical bacterial identification protocols were performed. They include catalase, carbohydrate fermentation, citrate utilisation, hydrogen sulphide production, and methyl red tests. Others were indole, methyl red, oxidase, Voges-Proskauer, motility and urease tests.

## 5. Results and discussion

### 5.1. Evaluation of the in-situ dose rate for the polluted coastlines

The gamma-absorbed dose rate was measured in situ using an RS-125 gamma spectrometer to evaluate the radiological risks associated with contaminated coastlines. The regional distribution of the gamma radiation

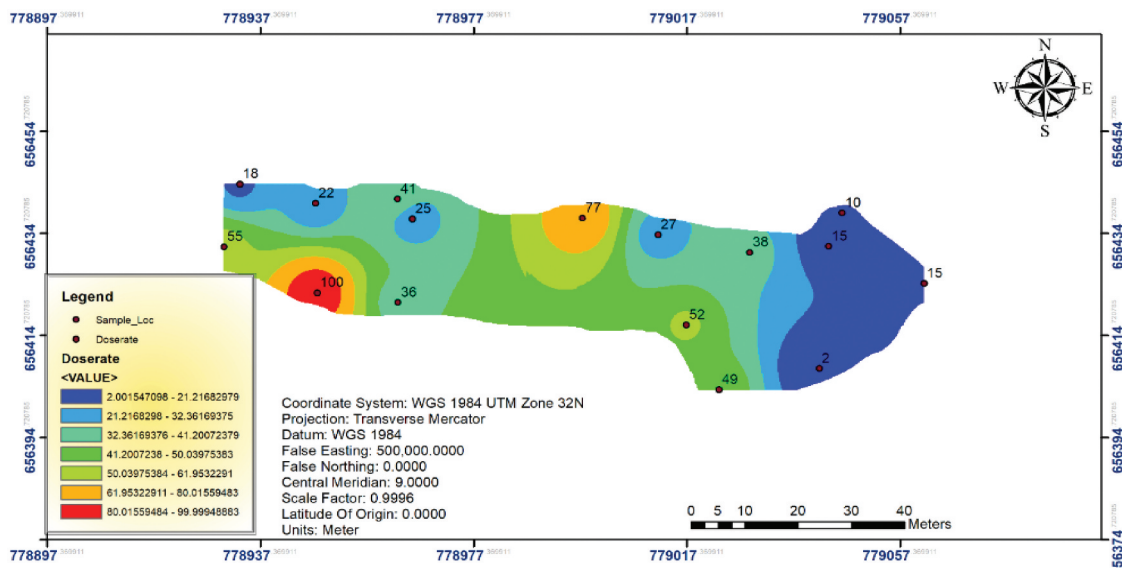


**Figure 3.** Spatial distribution of in-situ measured dose rate.

rates recorded in situ is shown in Figure 3. The locations 4 and 15 of the study area had the highest and lowest values of the absorbed dose rate, measuring  $100\text{ nGy/h}$  and  $2\text{ nGy/h}$ , respectively. Therefore, compared to other places, position 4 has a higher risk of ionising radiation exposure. This higher number of  $100\text{ nGy/h}$  is significantly greater than the UNSCEAR-recommended limit of  $59.00$  and  $84.00\text{ nGy/h}$  (UNSCEAR, 2000).

### 5.2. Activities of $^{40}\text{K}$ , $^{238}\text{U}$ and $^{232}\text{Th}$ in the sediment, water and fish samples from the coastline using a $3 \times 3$ inch NaI(Tl) detector

Tables 2 to 4 and Figures 4 To Figure 7 summarise activity concentrations of  $^{238}\text{U}$ ,  $^{232}\text{Th}$ , and  $^{40}\text{K}$  in

contaminated seashore sediments, waters, and fish. Results show a skewed distribution of primordial radionuclides due to asymmetry in their probability distribution (Normality Testing, Skewness and Kurtosis, 2019). The high standard deviations indicate that the results are spread out over a large range of values. The variance also reveals that the results are very spread out from the mean and from one another.

For the sediments and waters from the polluted coastlines, the minimum values of the activity concentrations of  $^{40}\text{K}$ ,  $^{238}\text{U}$ , and  $^{232}\text{Th}$  were  $102.23$ ,  $54.24$ ,  $47.65$  and  $126.71$ ,  $39.43$ ,  $60.24\text{ Bq kg}^{-1}$ , respectively, according to Tables 2 and 3. The corresponding higher values are  $288.09$ ,  $96.49$ ,  $136.12$  and  $257.307$ ,  $66.93$ ,  $96.57\text{ Bq kg}^{-1}$ , respectively. The

**Table 2.** Activities of  $^{40}\text{K}$ ,  $^{238}\text{U}$  and  $^{232}\text{Th}$  in the sediment samples from the coastline using  $3 \times 3$  inch NaI [TI] Gamma Spectroscopy Analysis.

S/No.	Sample ID	$^{40}\text{K}$ (Bq/kg)	$^{238}\text{U}$ (Bq/kg)	$^{232}\text{Th}$ (Bq/kg)
1	S1	$224.433 \pm 1.3407$	$83.4699 \pm 4.8348$	$105.768 \pm 2.3198$
2	S2	$242.237 \pm 1.5016$	$74.999 \pm 0.3596$	$47.6546 \pm 2.0053$
3	S4	$106.13 \pm 1.877$	$54.9007 \pm 2.0778$	$76.2395 \pm 1.0616$
4	S3	$184.534 \pm 1.2871$	$60.8942 \pm 1.1188$	$109.464 \pm 0.7864$
5	S5	$252.695 \pm 1.877$	$80.6329 \pm 1.5184$	$84.6931 \pm 1.3368$
6	S7	$194.723 \pm 2.6278$	$72.7614 \pm 2.7171$	$79.5816 \pm 0.0786$
7	S9	$137.609 \pm 2.3596$	$76.2377 \pm 0.04$	$136.122 \pm 0.4718$
8	S8	$259.023 \pm 1.3943$	$71.8424 \pm 1.9579$	$76.5934 \pm 2.7916$
9	S6	$239.931 \pm 2.306$	$58.2571 \pm 1.9179$	$103.212 \pm 2.2805$
10	S11	$280.313 \pm 0.9117$	$96.4958 \pm 1.2387$	$104.864 \pm 1.9266$
11	S10	$288.089 \pm 2.5741$	$57.2981 \pm 1.6382$	$92.0851 \pm 2.7523$
12	S12	$116.141 \pm 1.2091$	$59.2421 \pm 0.028$	$132.123 \pm 0.2115$
13	S14	$182.722 \pm 2.9922$	$65.5224 \pm 1.7672$	$66.7231 \pm 1.2414$
14	S13	$190.211 \pm 1.5214$	$54.2461 \pm 1.5827$	$103.212 \pm 1.2907$
15	S15	$102.231 \pm 1.0321$	$83.4368 \pm 1.0315$	$104.864 \pm 1.9266$
16	S_Control	$91.3441 \pm 0.1322$	$46.2321 \pm 0.0364$	$37.0851 \pm 0.1323$
	Min	102.2310	54.2461	47.6546
	Max	288.0892	96.4958	136.1224
	Mean $\pm$ SD	$200.0682 \pm 62.3369$	$70.0158 \pm 12.6663$	$94.8800 \pm 23.6160$
	Median	194.7230	71.8424	103.2124
	Mode	#N/A	#N/A	103.2124
	Variance	3885.8938	160.4351	557.7131
	Kurtosis	-1.1365	-0.5592	0.0487
	Skewness	-0.3090	0.4806	-0.0973



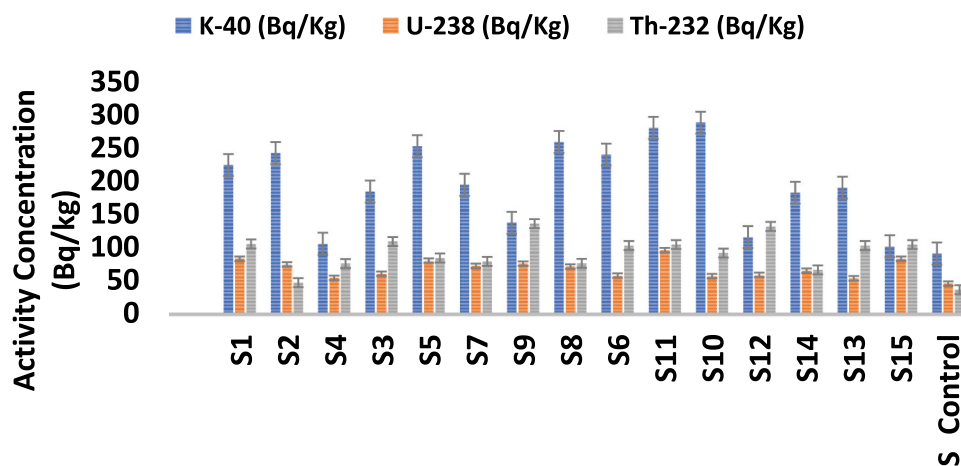


**Figure 4.** Activities of  $^{40}\text{K}$ ,  $^{238}\text{U}$  and  $^{232}\text{Th}$  in the water sample from the costline using  $3\times 3$ inch NaI [TL] gamma spectroscopy Analysis.

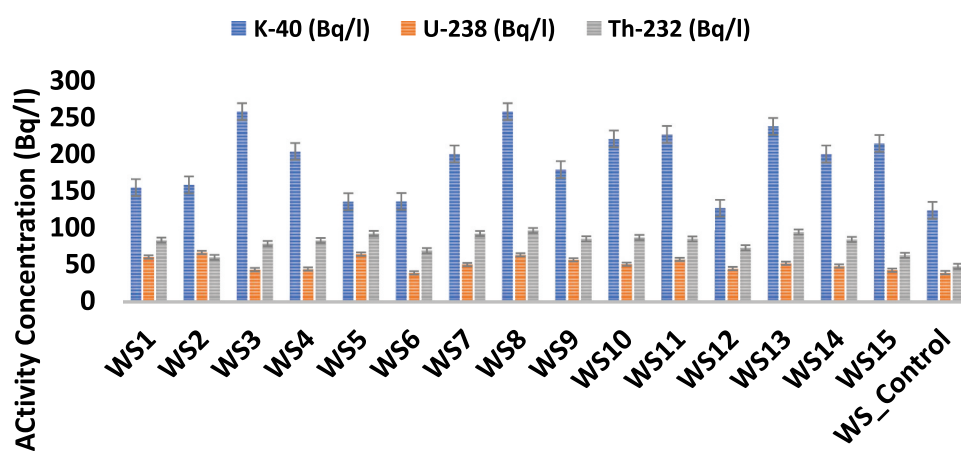


**Figure 5.** Activities of  $^{40}\text{K}$ ,  $^{238}\text{U}$  and  $^{232}\text{Th}$  in the water sample from the costline using  $3\times 3$ inch NaI [TL] gamma spectroscopy Analysis.

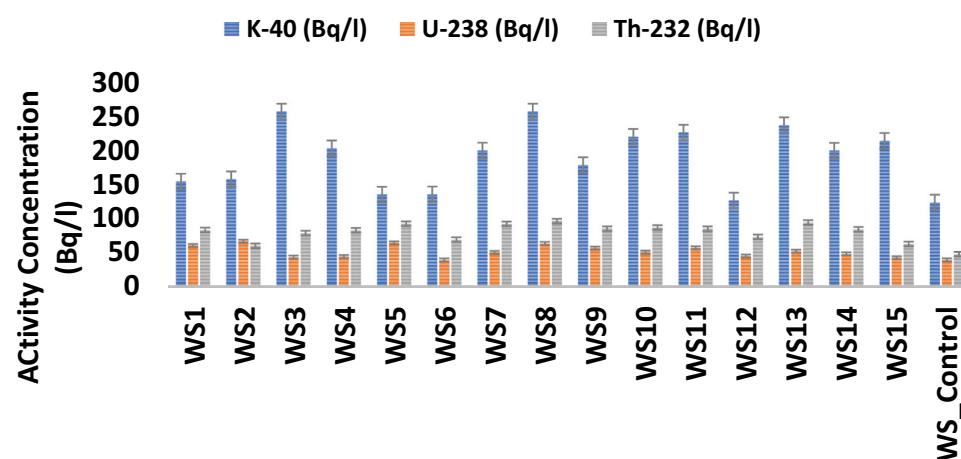


**Figure 6.** Activities of  $^{40}\text{K}$ ,  $^{238}\text{U}$  and  $^{232}\text{Th}$  in the water sample from the costline using  $3\times 3$ inch NaI [TL] gamma spectroscopy Analysis.

estimated mean values of these measured activities of  $^{40}\text{K}$ ,  $^{238}\text{U}$  and  $^{232}\text{Th}$  for the sediment and water are  $200.07 \pm 62.34$ ,  $70.02 \pm 12.67$ ,  $94.88 \pm 23.62$  and  $193.73 \pm 43.60$ ,  $52.59 \pm 8.75$ ,  $82.00 \pm 11.10 \text{ Bqkg}^{-1}$ , respectively. It was found that the average activity concentration of  $^{40}\text{K}$  in both the sediment and the

water was less than the  $420.00 \text{ Bqkg}^{-1}$  tolerable threshold (UNSCEAR, 2000). However, according to data from the ICRP (1991), International Atomic Energy Agency (IAEA) (1996) and (UNSCEAR, 2000), the mean activity of  $^{238}\text{U}$  and  $^{232}\text{Th}$  for both sediment and water were found to be higher than the

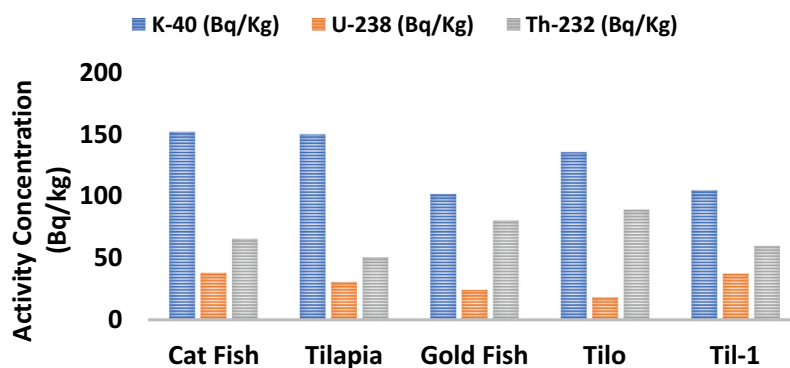


**Figure 7.** Activities of  $^{40}\text{K}$ ,  $^{238}\text{U}$  and  $^{232}\text{Th}$  in the water sample from the coastline using 3×3inch NaI [TL] gamma spectroscopy Analysis.

**Table 3.** Activities of  $^{40}\text{K}$ ,  $^{238}\text{U}$  and  $^{232}\text{Th}$  in the water samples from the coastline using 3 x 3 inch NaI [TI] Gamma Spectroscopy Analysis.

S/No.	Sample ID	$^{40}\text{K}$ (Bq/kg)	$^{238}\text{U}$ (Bq/kg)	$^{232}\text{Th}$ (Bq/kg)
1	WS1	154.609 ± 2.7887	60.8143 ± 2.0778	83.5529 ± 2.1625
2	WS2	158.149 ± 1.5552	66.9277 ± 1.6382	60.2367 ± 1.1009
3	WS3	257.307 ± 2.1451	43.7927 ± 2.1177	78.9525 ± 0.7864
4	WS4	203.411 ± 0.4827	44.5918 ± 1.3985	83.1204 ± 1.73
5	WS5	135.518 ± 1.7697	64.6502 ± 2.9168	92.6749 ± 0.0786
6	WS6	135.732 ± 1.7161	39.4374 ± 0.3996	69.3587 ± 3.0669
7	WS7	200.086 ± 1.5552	50.5454 ± 2.0778	92.4783 ± 1.6121
8	WS8	257.307 ± 2.1451	63.6912 ± 1.1188	96.5675 ± 2.0446
9	WS9	178.849 ± 1.2871	56.9385 ± 2.3575	85.3615 ± 2.0053
10	WS10	220.25 ± 2.4133	50.9849 ± 1.9579	87.0916 ± 3.8139
11	WS11	226.417 ± 2.3596	57.4579 ± 0.919	85.2436 ± 0.7864
12	WS12	126.711 ± 1.4231	45.1674 ± 0.5626	73.3217 ± 3.7462
13	WS13	237.301 ± 2.1131	52.3212 ± 1.1142	94.5136 ± 2.0216
14	WS14	200.001 ± 1.4212	48.5421 ± 2.0113	84.4513 ± 1.142
15	WS15	214.237 ± 2.0031	42.9154 ± 1.8237	63.0776 ± 3.0029
16	WS_Control	123.813 ± 0.1001	39.6525 ± 1.0015	48.1287 ± 1.0021
	Min	126.7113	39.4374	60.2367
	Max	257.3068	66.9277	96.5675
	Mean	193.7257 ± 43.5972	52.5852 ± 8.7455	82.0002 ± 11.1036
	Median	200.0858	50.9849	84.4513
	Mode	257.3068	#N/A	#N/A
	Variance	1900.7131	76.4830	123.2909
	Kurtosis	-1.1817	-1.2100	-0.3035
	Skewness	-0.1402	0.2437	-0.7311

**Table 4.** Activities of  $^{40}\text{K}$ ,  $^{238}\text{U}$  and  $^{232}\text{Th}$  in the Fish samples from the coastline using 3 x 3 inch NaI [TI] Gamma Spectroscopy Analysis.

S/No.	Sample ID	$^{40}\text{K}$ (Bq/kg)	$^{238}\text{U}$ (Bq/kg)	$^{232}\text{Th}$ (Bq/kg)
1	Cat Fish	151.874	37.999	65.5054
2	Tilapia	149.783	30.6069	50.7215
3	Gold Fish	101.571	24.2538	80.368
4	Tilo	135.411	18.3801	89.0182
5	Til-1	104.789	37.3197	59.7649

corresponding global average values of 32.00 and 45.00  $\text{Bqkg}^{-1}$ , respectively.

The various mean concentrations of the primordial radionuclides from one species of fish to another are displayed in Table 4 and Figure 6. Catfish, one of the fish species collected in the study area, had higher mean concentrations of  $^{40}\text{K}$  and  $^{238}\text{U}$ , with 151.87 and 38.00  $\text{Bqkg}^{-1}$ , respectively. On the other hand, Tilo had greater mean  $^{232}\text{Th}$  activity, measuring 89.02  $\text{Bqkg}^{-1}$ . These differences are not unrelated to species specialisation determined by metabolism and feeding patterns. Metabolic activity and eating habits are two of

the most important aspects that contribute significantly to the build-up of hazardous elements in aquatic animals.

### 5.3. Analysis of the radiological hazard

Tables 5, Tables 6 and 7 present the estimated radioactive indices for the waters, fish, and sediments from the contaminated coastline. The average absorbed dose rates for the sediments are 184.79  $\text{nGy/h}$  indoors and 97.86  $\text{nGy/h}$  outdoors, respectively. Additionally, these mean values exceed the suggested limitations of

**Table 5.** Radiation hazard indices for sediments derived from contaminated coastal areas.

Points	$D_{in}$ ( $nGyh^{-1}$ )	$D_{out}$ ( $nGyh^{-1}$ )	$AED_{out}$ ( $mSvy^{-1}$ )	$AED_{in}$ ( $mSvy^{-1}$ )	$Ra_{eq}$ ( $Bqkg^{-1}$ )	$H_{ext}$	$H_{int}$	RLI	ELCR	AGED ( $mSvy^{-1}$ )
S1	211.09	111.65	0.14	1.04	252.00	0.68	0.91	1.77	3.62	0.77
S2	140.80	73.36	0.09	0.69	161.80	0.44	0.64	1.14	2.42	0.51
S4	142.86	75.76	0.09	0.70	172.10	0.47	0.62	1.20	2.45	0.52
S3	191.20	101.82	0.12	0.94	231.64	0.63	0.79	1.63	3.28	0.70
S5	187.56	98.77	0.12	0.92	221.20	0.60	0.82	1.56	3.22	0.68
S7	170.06	89.67	0.11	0.83	201.56	0.55	0.74	1.41	2.92	0.62
S9	230.88	123.08	0.15	1.13	281.49	0.77	0.97	1.96	3.96	0.85
S8	171.07	90.07	0.11	0.84	201.32	0.55	0.74	1.42	2.94	0.62
S6	186.32	99.09	0.12	0.91	224.33	0.61	0.77	1.58	3.20	0.69
S11	226.55	119.41	0.15	1.11	268.04	0.73	0.99	1.88	3.89	0.82
S10	177.05	93.90	0.12	0.87	211.16	0.57	0.73	1.50	3.04	0.65
S12	209.13	111.93	0.14	1.03	257.12	0.70	0.86	1.80	3.59	0.77
S14	148.29	78.06	0.10	0.73	175.01	0.48	0.65	1.23	2.55	0.54
S13	178.66	95.20	0.12	0.88	216.49	0.59	0.74	1.52	3.07	0.66
S15	200.29	106.08	0.13	0.98	241.26	0.66	0.88	1.68	3.44	0.73
$S_{Control}$	90.63	47.50	0.06	0.44	106.30	0.29	0.41	0.74	1.56	0.33
Min	140.80	73.36	0.09	0.69	161.80	0.44	0.62	1.14	2.42	0.51
Max	230.88	123.08	0.15	1.13	281.49	0.77	0.99	1.96	3.96	0.85
Mean	184.79	97.86	0.12	0.91	221.10	0.60	0.79	1.55	3.17	0.68
Acceptable LIMIT	84.00	59.00	0.07	0.41	370.00	$\leq 1$	$\leq 1$	$\leq 1$	3.75	0.30

**Table 6.** Hazard indices of waters from the contaminated shorelines.

Points	$AED_{ing}$ ( $mSvy^{-1}$ )	$Ra_{eq}$ ( $Bqkg^{-1}$ )	$H_{ext}$	$H_{int}$	ELCR ( $\times 10^{-3}$ )	AGED ( $mSvy^{-1}$ )
WS1	0.2593	192.1999	0.5225	0.6867	0.9074	0.5857
WS2	0.2019	165.2436	0.4488	0.6295	0.7068	0.5083
WS3	0.2458	176.5074	0.4802	0.5984	0.8604	0.5461
WS4	0.2533	179.1166	0.4873	0.6077	0.8865	0.5491
WS5	0.2836	207.6102	0.5644	0.7390	0.9926	0.6297
WS6	0.2101	149.0717	0.4055	0.5120	0.7354	0.4544
WS7	0.2804	198.1960	0.5392	0.6756	0.9816	0.6056
WS8	0.3018	221.5953	0.6026	0.7746	1.0563	0.6813
WS9	0.2637	192.7768	0.5242	0.6779	0.9229	0.5889
WS10	0.2681	192.4851	0.5236	0.6612	0.9382	0.5907
WS11	0.2670	196.7904	0.5351	0.6903	0.9344	0.6050
WS12	0.2227	159.7742	0.4345	0.5565	0.7795	0.4858
WS13	0.2893	205.7478	0.5597	0.7010	1.0124	0.6313
WS14	0.2585	184.7075	0.5024	0.6335	0.9048	0.5658
WS15	0.2010	149.6126	0.4069	0.5227	0.7036	0.4635
$WS_{Control}$	0.1541	118.0101	0.3208	0.4278	0.5394	0.3626
Min	0.2010	149.0717	0.4055	0.5120	0.7036	0.4544
Max	0.3018	221.5953	0.6026	0.7746	1.0563	0.6813
Mean	0.2538	184.7623	0.5025	0.6444	0.8882	0.5661
Acceptable LIMIT	1.00	370.00	$\leq 1$	$\leq 1$	3.75	0.30

**Table 7.** Radiological hazard indices for the fishes from the polluted coastlines.

Sample Type	$AED_{ing}$ ( $mSvy^{-1}$ )	$Ra_{eq}$ ( $Bqkg^{-1}$ )	$H_{ext}$	$H_{int}$	ELCR ( $\times 10^{-3}$ )	AGED ( $mSvy^{-1}$ )
Cat Fish	0.2005	143.3660	0.3900	0.4926	0.7017	0.4389
Tilapia	0.1581	114.6719	0.3119	0.3945	0.5533	0.3536
Gold Fish	0.2286	147.0010	0.4003	0.4657	0.8002	0.4428
Tilo	0.2505	156.1027	0.4252	0.4749	0.8768	0.4714
Til-1	0.1819	130.8523	0.3559	0.4566	0.6366	0.3980
Acceptable LIMIT	1.00	370.00	$\leq 1$	$\leq 1$	3.75	0.30

59.00 and 84.00  $nGy/h$ , respectively (UNSCEAR, 2000). Consequently, these contaminated coastlines have a higher risk of ionising radiation exposure. The highest and lowest yearly effective doses, respectively, for outdoor and indoor environments are 0.09 and 0.15  $mSv/y$  and 0.69 and 1.13  $mSv/y$ . Furthermore, both the indoor and outdoor mean values of yearly effective doses exceed the recommended standards of 0.41 and 0.07  $mSv/y$  (UNSCEAR, 2000). The RLI trended in the same direction, with values exceeding the recommended limit of 1. Thus, it's possible that sediments

from coastlines aren't appropriate for construction. In addition, similar observations are recorded for the water samples. The mean  $AED_{ing}$  due to ingestion of the radionuclides in the water is 0.2538  $mSv/y$ . This mean value, however, is lower than the UNSCEAR-recommended threshold of 1.00  $mSv/y$  (UNSCEAR, 2000). Corroborating our previous findings, the calculated average values of  $Ra_{eq}$ ,  $ELCR$ ,  $H_{ext}$ ,  $H_{int}$ , and  $AGED$  also follow suit. All of the fish hazard indices estimated mean values, however, fell within the appropriate recommended ranges.

#### 5.4. Microbial analysis and bioaccumulation

The microbiological assessment revealed bacterial and fungal isolates. The sediment samples labelled SS2, SS4, SS5 and SS8 reported Gram-negative isolates of *Escherichia coli* and *Pseudomonas aeruginosa* and Gram-positive isolates of *Staphylococcus* and *Bacillus* species, respectively. Water samples SW1 and SW5 showed the presence of Gram-positive *Bacillus* species, and Gram-negative *Escherichia coli*, respectively. The biochemical characteristics that aided the identification of bacterial isolates are also presented in Table 8. *Escherichia* species were identified by their positive reactions to motility, glucose, lactose, and mannitol utilisation as well as indole, methyl red, and catalase tests; while *Pseudomonas aeruginosa* reacted negatively to maltose and indole tests, and positively to the other biochemical tests. Conversely, *Staphylococcus* species were negative to motility, Voges Proskauer, H<sub>2</sub>S production, and oxidase tests; while *Bacillus* species were identified by their negative reactions to methyl red, urea, and oxidase tests. The Gram-positive isolates gave a positive reaction to the other biochemical tests and were distinguished by their cocci and bacilli shapes upon observation under the microscope. Likewise, Table 9 shows the microscopic and cultural characteristics of the fungal isolates of the *Mucor* and *Aspergillus* genera obtained from both the sediment and water samples. *Mucor* species isolated from samples SS1, SS4, and SW2 were identified by the blackish zygomycetes showing a fluffy white edge on the culture plates; and the observed non-septate and darkly pigmented spores during microscopy. The *Aspergillus* species isolated from samples SS8, SW5 and SW9 presented numerous black spores and a brownish-grey colouration on the reverse side of the culture plates, while the microscopy revealed large rough-walled conidia possessing a globose loose column. However, they had smooth-walled and biseriate conidiophores with septate phialides. This microbial community is a diverse group of aerobic organotrophs and fermentative and denitrifying microorganisms, despite being sparse.

The bacterial counts in colony-forming units per gram (CFU/g) of the sediment samples (Table 10) were  $1.7 \times 10^3$  (*Escherichia coli*),  $2.0 \times 10^3$  (*Pseudomonas* sp.),  $2.6 \times 10^3$  (*Staphylococcus aureus*) and  $8.8 \times 10^3$  (*Bacillus* sp). The fungal counts in colony-forming units per gram (CFU/g) of the sediment samples were  $0.1 \times 10^3$  (*Mucor* sp. at SS1),  $0.2 \times 10^3$  (*Aspergillus* sp. at SS8), and  $0.4 \times 10^3$  (*Mucor* sp. at SS4). In the same vein, the bacterial counts in colony-forming units per millilitre (CFU/ml) of the water samples (Table 11) were  $2.0 \times 10^3$  (*Bacillus* sp.) and  $4.0 \times 10^3$  (*Escherichia coli*), while the fungal counts were  $0.6 \times 10^3$  (*Mucor* sp.),  $0.4 \times 10^3$  (*Aspergillus* sp. at SW5),

and  $1.4 \times 10^3$  *Aspergillus* sp. at SW9 sampled at location 9. With microbial interactions thought to influence the speciation, mobility, and migration behaviour of radionuclides (Gerber et al., 2016), the *Bacillus*, *Pseudomonas*, and *Aspergillus* isolated at the study sites corroborate the studies of Ding et al. (2012) and Gerber et al. (2016). The authors reported the potency of indigenous microorganisms of the genera *Pseudomonas*, *Bacillus*, and *Aspergillus* to immobilise U(VI) as uranyl phosphate minerals.

As with any contaminated front, the presence of radioactive wastes would lead to changes in physico-chemical characteristics and other aquatic components (Abdissa & Beyecha, 2021; Møller & Mousseau, 2013; Nguyen et al., 2021). From the observed results, location 9 showed high activities of <sup>238</sup>U and <sup>232</sup>Th, which matched the area showing maximum values of the outdoor and indoor absorbed dose rates of 54.03 and 102.77 nGy/h, respectively. Moreover, despite these observed results falling within recommended limits, the presence of the primordial radionuclides (<sup>238</sup>U, <sup>232</sup>Th and <sup>40</sup>K) calls for concern; Li et al. (2014) and Liu et al. (2023) opines that uranium results in serious biological and chemical toxicity and high radioactivity. Nazina et al. (2010) found that these changes will vary depending on the hydrodynamic connection at the point of radioactive waste discharge and the overall water body. Other factors include organic matter, nitrates, sulphates, oxidised forms of radionuclides, and other metals accompanying the waste, including bicarbonates, which were initially present at the site (Xiong et al., 2022; Yuan et al., 2023; Zhou et al., 2023). Molecular hydrogen, probably formed by water radiolysis at the disposal site, could also be a factor. Considering also that for both sediment and water, the mean values of the activity concentration of <sup>40</sup>K were below the acceptable threshold, while <sup>238</sup>U and <sup>232</sup>Th were above their corresponding threshold values, the aforementioned background factors might have influenced microbial life. According to the reports of Zhao et al. (2016), these may account for possible selective substrates for microbial metabolism that allowed for the sparse bacterial and fungal presence reported at the site of contamination. It is noteworthy, however, that microbial interactions with radioactive contaminants come by different mechanisms, such as biosorption, bioaccumulation within the cell, reduction, and biomineralization (Sousa et al., 2013; Tu et al., 2019; Zhang et al., 2021).

Overall, the results of this study showed an even distribution of gram-positive and gram-negative bacteria, contrary to the largely gram-negative bacterial population dominant in the groundwater, as submitted by Stroes-Gascoyne et al. (2011). Of particular significance in this study is the presence of *Pseudomonas*, *Staphylococcus*, and *Bacillus* genera reported to be associated with denitrification of

**Table 8.** Gram reaction and biochemical characteristics of bacterial isolates from sediment and water samples

Sample Source	Sample label	Gram Reaction	Motility	Glucose	Lactose	Mannitol	Maltose	Indole	Methyl Red	Voges Proskauer	Citrate	H <sub>2</sub> S	Sucrose	Urea	Oxidase	Coagulase	Catalase	Probable Organism
Sediment	SS2	GNB	+	+	+	+	+	+	+	-	-	-	NA	-	-	NA	+	<i>Escherichia</i> sp
	SS4	GNB	+	+	-	-	-	-	+	+	+	+	+	+	+	NA	+	<i>Pseudomonas aeruginosa</i>
	SS5	GPC	-	+	+	+	+	NA	+	-	+	-	+	+	-	+	+	<i>Staphylococcus</i> sp
	SS8	GPB	+	+	+	+	+	NA	-	+	NA	NA	+	-	-	NA	+	<i>Bacillus</i> sp
Water	SW1	GPB	+	+	+	+	+	NA	-	+	NA	NA	+	-	-	NA	+	<i>Bacillus</i> sp
	SW5	GNB	+	+	+	+	+	+	+	-	-	-	NA	-	-	NA	+	<i>Escherichia</i> sp

\*NA = Not applicable; GNB = Gram negative bacilli; GPC = Gram positive cocci; GPB = Gram positive bacilli.

**Table 9.** Macroscopic and Microscopic characteristics of fungal isolates from sediment and water samples

Sample Source	Sample label	Macroscopy	Microscopy	Probable Organism
Sediment	SS1	Blackish zygomycetes with a fluffy white edge	Zygomycete with non-septate hyphae; sporangia are slimy in texture and the spores have a dark pigment.	<i>Mucor</i> sp.
	SS4	Blackish zygomycetes with a fluffy white edge	Zygomycete with non-septate hyphae; sporangia are slimy in texture and the spores have a dark pigment	<i>Mucor</i> sp.
	SS8	Numerous black spores with a reverse brownish grey colouration	Large rough-walled conidia that are globose with loose column. Conidiophores are smooth-walled and biserial with septate phialides.	<i>Aspergillus</i> sp.
Water	SW2	Blackish zygomycetes with a fluffy white edge	Zygomycete with non-septate hyphae; sporangia are slimy in texture and the spores have a dark pigment.	<i>Mucor</i> sp.
	SW5	Numerous black spores with a reverse brownish grey colouration	Large rough-walled conidia that are globose with loose column. Conidiophores are smooth-walled and biserial with septate phialides.	<i>Aspergillus</i> sp.
	SW9	Numerous black spores with a reverse brownish grey colouration	Large rough-walled conidia that are globose with loose column. Conidiophores are smooth-walled and biserial with septate phialides.	<i>Aspergillus</i> sp.

**Table 10.** Isolate counts from sediment samples.

Sample label	Probable organism	Count (CFU/g)
SS1	<i>Mucor</i> sp	$0.1 \times 10^3$
SS2	<i>Escherichia coli</i>	$1.7 \times 10^3$
SS4	<i>Pseudomonas aeruginosa</i>	$2.0 \times 10^3$
	<i>Mucor</i> sp	$0.4 \times 10^3$
SS5	<i>Staphylococcus aureus</i>	$2.6 \times 10^3$
SS8	<i>Bacillus</i> sp	$8.8 \times 10^3$
	<i>Aspergillus</i> sp	$0.2 \times 10^3$

\*CFU = Colony forming units per gram.

**Table 11.** Isolate counts from water samples.

Sample label	Probable organism	Count (CFU/ml)
SW1	<i>Bacillus</i> sp	$2.0 \times 10^3$
SW2	<i>Mucor</i> sp	$0.6 \times 10^3$
SW5	<i>Escherichia coli</i>	$4.0 \times 10^3$
	<i>Aspergillus</i> sp	$0.4 \times 10^3$
SW9	<i>Aspergillus</i> sp	$1.4 \times 10^3$

\*CFU = Colony forming units per millilitre

organic pollutants and the attendant production of free nitrogen (Tu et al., 2019; Plymale, et al., 2021). *Pseudomonadales* are reported to have a high capacity for biosorption of various radionuclides (Lazareva et al., 2011). These *Bacillus* and *Pseudomonas* species of microorganisms could be attributed to the biogenic precipitation and concentration of radionuclides in the disposal sites compared with previous studies (Tu et al., 2019; Plymale, et al., 2021); as such, they may be potentially hazardous to exposure to aquatic lives (Wang et al., 2019). In addition, the interactions of biogenic precipitation and radioactivity concentrations in such an environment may degenerate to bioaccumulation and biomagnification in the survival of aquatic lives, which poses a threat to the health of humans that consume fishes and other seafood (Lazareva et al., 2011; Møller & Mousseau, 2013; Tu et al., 2019).

In all cases for this study, considering Table 10, the number of microorganisms did not exceed  $10^3$  cells per gram or millilitre of sediment and water samples. However, the average bacterial count was higher than the fungal count. The reports of Sarro et al. (2005) and Rivasseau et al. (2016) that focused on spent nuclear

fuel storage pools identified microorganisms after cultivation, but with a huge loss in diversity, since only 0.1 to 10% of the microorganisms present in water are culturable (Stokell & Steck, 2012). This low microbial presence and counts could be attributable to the loss by some organisms of their culturability on appropriate media under certain stress conditions while retaining viability through greatly reduced metabolic activity. According to Stroes-Gascoyne et al. (2011), this viable but nonculturable (VBNC) effect may be due to bacterial spore formation, which is responsible for the stages in cell resistance to environmental changes. Previous studies indicate that these variations in stages may also solidify the cell wall, alter the fatty acid structure of the cell wall and alter the membrane cytoplasmic configuration. These structural changes reduce the genetic material within the cell, as such, enhances red tides that cause ecological marine disasters of invasion of pathogenic microorganisms' exposure to the marine fisheries. These structural stages and processes can affect the marine water environment and can lead to the death of the fishes found in the study area. In addition, the materials being transported in marine water can alter the food chain and may considerably alter the biogeochemistry of the marine sediments on which seafood relies. This condition of water-sediment biogeochemistry change could marginally affect the fishes marginally or greatly not both.

The loss of cytoplasmic membrane permeability causes culturability in VBNC cells. There are two phases: initial transition with culturability, followed by gradual degradation of RNA and DNA, leading to cell death. While some VBNC cells may have metabolic activity, the physiological basis for entry and exit is still under study (McDougald et al., 1998; Petit et al., 2020; Stokell & Steck, 2012). Proper evaluation of interactions between radionuclides, mineral surfaces, pore water, waste components, and diverse microbial species is crucial for understanding microorganism roles in

liquid radioactive waste sites. Moreover, the transport materials that interact with marine sediments may constitute radionuclides that can enhance red tides, which assimilate some of the nutrients, thus enhancing dissolved oxygen at the initial contact. These water-sediment-transport material interactions could heavily reduce the dissolved oxygen after a while which may affect the transformation of nutrients, productivity, and sedimentation of chlorophyll that aquatic life depends on since some species of chlorophyll are harmful to fishes. These processes of food chain alterations and transportation of waste materials may have reduced the biomass of living organisms at the peak level, which distorts the carbon transformation, resulting in the possible death of the fishes.

Microbial processes at the sediment-water interface may significantly influence the degradation, mobility, and migration of radionuclides in these environments. As described by Lopez-Fernandez et al. (2018), Microbial effects on clay, soils, and sediments involve dissolution of structural minerals, alteration of mineral surfaces, and formation of biofilms. Microbes control radionuclide speciation and mobility through processes like biosorption, intracellular accumulation, and biomineralization (Brookshaw et al., 2012; Newsome et al., 2014).

An apt example is the biomineralization of uranium resulting in the formation of U(VI) phosphate mineral phases, probably due to the activity of acid or alkaline phosphatases (Lütke et al., 2013). Salome et al. (2013) also reported the effect of uranium addition on the microbial diversity of sediment microcosms. Conversely, the studies of Law et al. (2010) and Roh et al. (2015) suggest that indigenous microbial communities have viewed these biotransformation activities of anthropogenic radionuclides as a potential mechanism for the sequestration and bioremediation of environmental radionuclide contamination.

Fishes primarily accumulate radioactive elements through ingestion, except for organisms with a large surface-to-volume ratio adapted for adsorption to surfaces (Lerebours et al., 2018). Catfish had the highest mean concentrations of  $^{238}\text{U}$  and  $^{40}\text{K}$  in the fish understudy, whereas tilapia had the highest mean activity of  $^{232}\text{Th}$ . By doing this, we hypothesise that the eating habits of the fish and the aquatic species, in conjunction with microbiological process mentioned above that lead to the radioactive speciation and mobility, will facilitate the entry and concentration of radionuclides into the food chain or web. This is because most of the radioactive materials likely to accumulate would actually biomagnify through these invertebrates via the different kinds of organisms that serve as their food. Generally, the factors that influence the bioaccumulation of toxicants by aquatic biota are grouped into intrinsic and extrinsic factors. The main extrinsic factor is the physico-chemical

properties of the ambient environment, i.e. water and sediment; exposure duration, concentration of toxicants, nearness to the source of pollution, among others. Intrinsic factors include the route of uptake (Yu et al., 2024), the age and size of the organism, and most importantly, the unique characteristics of the species, such as feeding habit and octanol/water partition coefficient. In the current study, the experimental fish species exhibited varied accumulation capacities, partly due to the differences in feeding habits and repository capacities. *Clarias gariepinus* is a benthopelagic feeder, with lipid content for storage of chemicals accumulated from the bottom of the aquatic environment. Hence, among the investigated fish species, *C. gariepinus* is culpable for future health hazards among consumers. Furthermore, the hardiness of the species keeps it alive even at dangerous concentrations of accumulation that may be lethal to other organisms. These factors, coupled with the relatively high commercial value due to the demands, mark the fish as a notable bioindicator against prognostic health concerns. Another factor in the concentration of radionuclides by aquatic organisms about which there is a dearth of information is the competition for uptake among chemicals. As such, concentration and specific activity could be strongly influenced by abiotic factors such as ions, pH, and other background elements present in the water (Beresford et al., 2016; Lopez-Fernandez et al., 2018; Shen et al., 2023; Zhang et al., 2020).

Studies suggest that any accumulation of radioactive materials in an organism is subject to biological dilution. Such dilutions result from cell division and growth, which is especially manifested in younger rapidly growing fishes. Upon maturity, there may be an inverse correlation between the complexity of body structure and the concentration of the radionuclides of interest. Thus, the observed mean concentrations were influenced at the time of this study. Other varying effects on these objects of fisheries or on their food might result in mortality induced by somatic effects or from genetic changes, which may be restricted to only the individual organism involved, or in some cases, the entire population. Isotopic dilutions, on the other hand, have a non-linear relationship but may be ineffective in instances where low concentrations occur (Beresford et al., 2016; Lerebours et al., 2018). It remains to be said if that is relatable to our study, location showed some mean concentrations within recommended limits with some outliers.

From the foregoing, the ability of the various organisms in the food web to concentrate radionuclides is of serious importance to predatory species and humans. If the animals, which serve as food to fishes or other seafood, were unable to take up the radionuclides, there would be considerably less

chance of the predators and man becoming contaminated. Unfortunately, the constraints on available information on the efficiency of transfer of particular radioisotopes from food organisms to aquatic predators remain a concern. Therefore, it is quite certain that the indirect hazard to humans through danger of contamination of food from aquatic environments will require limiting the permissible concentration of radioactive elements in the seas and oceans to levels much lower than those at which there could be any direct hazard.

## 6. Conclusion

The study evaluated biohazards and radioactive distributions in Unumherin village, Nigeria, using calibrated gamma detectors to measure outdoor dose rate and activity concentrations of  $^{40}\text{K}$ ,  $^{238}\text{U}$ , and  $^{232}\text{Th}$ . The laboratory examination of sediments, water, and fish from the same coastal region – *Clarias gariepinus*, *Pseudotropheus elongatus*, *Oreochromis niloticus* and *Stromateus fiatola* – was combined with the in-situ observations of gamma dose rates. With a value of 100 nGy/h, or nearly twice as high as the recommended limits, the hotspot at site 4 is shown by the geographic distribution of gamma dose rates. The findings demonstrated that the primordial radionuclides ( $^{40}\text{K}$ ,  $^{238}\text{U}$ , and  $^{232}\text{Th}$ ) exhibited a range of activities, with average values exceeding the suggested thresholds for both the sediments and the water. In the same way, values that were generally greater than the suggested limits were found in the radiation effect evaluations. The proposed allowable limit was not met by the estimated mean hazard indices for the sediments in the research area. All of the fish hazard indices projected mean values fell between the prescribed limits for each. *Clarias gariepinus*, having accumulated higher levels of most radionuclides investigated, is a suitable bioindicator for early warning signals of toxicity levels that may elicit health hazards in consumers. The accumulation of toxicants in the catfish species assessed is attributable to its dorsal/subterminal mouthpart, which confers its benthopelagic feeding habits. As a bottom feeder of the catfish, it is prone to toxicants that settle enormously in repository bottom sediment. The other fish species investigated have demersal feeding habits, characterised by terminal and supra-terminal mouthparts, hence relatively less exposure to contaminants than the catfish, which also has a high lipid content for storage of chemicals. The hardness of catfish makes it most likely to be alive even at concentrations that may be lethal to other species that are less resilient in the event of pollution. Varying mean concentrations, activities, and absorbed dose rates of the radionuclides

understudied account for the sparse but somewhat diverse bacterial and fungal presence reported at the site of contamination. This microbial community represented the various physiological groups of aerobic organotrophs and fermentative and denitrifying microorganisms. Microbial interactions with radioactive contaminants via biosorption, bioaccumulation within the cell, reduction and biomineralization could have culminated in varying mean concentrations of  $^{40}\text{K}$ ,  $^{238}\text{U}$ , and  $^{232}\text{Th}$  in the fish. Further reduction of the permissible concentrations of radioactive elements in aquatic environments as well as many of the lower plant and animal forms, such as bacteria, protozoa, and phytoplankton, would preclude any chances of direct and indirect hazards to humans.

## Acknowledgments

The Covenant University Centre for Research, Innovation, and Discovery (CUCRID) provided an atmosphere that allowed the authors to conduct this research, and for that the authors are grateful. We also acknowledge the support of the Unumherin Community in the Niger Delta for helping with the data collecting. Lastly, we express our gratitude to the Biotechnology and Radiation Geophysics Research Cluster for their invaluable assistance with every facet of this investigation. Dr. Oghenero Ohwoghre-Asuma has given us explicit permission to use and alter their map, which the writers greatly appreciate.

## Disclosure statement

No potential conflict of interest was reported by the author(s).

## ORCID

Muyiwa M. Orosun  <http://orcid.org/0000-0002-0236-3345>

## Authors contributions

**Omeje Maxwell:** Prepared the paper and data analysis, **Muyiwa M. Orosun:** Sample collection and measuring the sample proportion, **Aimua Godfrey:** Sampling and Sample collection, **Olusegun O. Adewoyin:** Assembled the materials for the study and data analysis, **Emmanuel S. Joel:** Data Curation, **Conrad A Omohinmin:** Editing the statistical analysis and proofreading of the article, **Eze F. Ahuekwe:** Microbiological analysis of the water and sediment samples, **Patrick O. Isibor:** Fish sample preparation and analysis, **Mojisola R. Usikalu:** Radioactivity analysis, **Oha A. Ifeanyi & Soheil Sabri:** GIS analysis, **Nuradeen N. Garba:** Data preparation, **Hitler Louis, Terkaa V. Targema & Soheil Sabri:** Suggestions, revision and proofreading of the article.

## Data availability statement

The data is available on request from the corresponding author.



## References

- Abbasi, A., & Mirekhtiary, F. (2020). Heavy metals and natural radioactivity concentration in sediments of the Mediterranean Sea coast. *Marine Pollution Bulletin*, 154, 111041. <https://doi.org/10.1016/j.marpolbul.2020.111041>
- Abdissa, D., & Beyecha, K. (2021). Sugarcane bagasse adsorption evaluation and application on BOD and COD removal from textile wastewater treatment. *WATER CONSERVATION & MANAGEMENT*, 5(1), 30–34. <https://doi.org/10.26480/wcm.01.2021.30.34>
- Abdulwahid, K. D. (2023). Phytoremediation of cadmium pollutants in wastewater by using *Ceratophyllum Demersum* L. as an Aquatic Macrophytes. *WATER CONSERVATION & MANAGEMENT*, 7(2), 83–88. <https://doi.org/10.26480/wcm.02.2023.83.88>
- Abosedo, O. B. (2020). *How oil and water create a complex conflict in the Niger Delta*. <https://theconversation.com/how-oil-and-water-create-a-complex-conflict-in-the-niger-delta-135105>
- Adagunodo, T. A., George, A. I., Ojoawo, I. A., Ojesanmi, K., & Ravisankar, R. (2018). Radioactivity and radiological hazards from a kaolin mining field in Ifonyintedo, Nigeria. *MethodsX*, 5, 362–374. <https://doi.org/10.1016/j.mex.2018.04.009>
- Adegoke, O. S., Oyebamiji, A. S., Edet, J. J., Osterloff, P. I., & Ulu, O. (Eds.). (2017). K Cenozoic Foraminifera and Calcareous. Nannofossil Biostratigraphy of the Niger Delta. In: *Part I: Cenozoic Foraminifera Biostratigraphy of the Niger Delta* (1st ed., pp. 386–394). Elsevier. <https://doi.org/10.1016/B978-0-12-812161-0.00007-7>
- Ahmad, H. A., Ahmad, S., Gao, L., Ismail, S., Wang, Z., El-Baz, A., & Ni, S. (2023). Multi-omics analysis revealed the selective enrichment of partial denitrifying bacteria for the stable coupling of partial-denitrification and anammox process under the influence of low strength magnetic field. *Water Research*, 245, 120619. <https://doi.org/10.1016/j.watres.2023.120619>
- Ajibola, T. B., Orosun, M. M., Ehinlafa, O. E., Sharafudeen, F. A., Salawu, B. N., Ige, S. O., & Akoshile, C. O. (2022). Radiological hazards associated with 238U, 232Th, and 40K in some selected packaged drinking water in Ilorin and Ogbomoso, Nigeria. *Pollution*, 8(1), 117–131.
- Akpoborie, I. A., Aweto, K. E., & Ohwoghre-Asuma, O. (2015). Urbanization and Major Ion Hydrogeochemistry of the shallow aquifer at the Effurun - Warri Metropolis, Nigeria. *Environment and Pollution*, 4(1). <https://doi.org/10.5539/ep.v4n1p37>
- Beresford, N. A., Fesenko, S., Konoplev, A., Skuterud, L., Smith, J. T., & Voigt, G. (2016). Thirty years after the Chernobyl accident: What lessons have we learnt? *Journal of Environmental Radioactivity*, 157, 77–89. <https://doi.org/10.1016/j.jenvrad.2016.02.003>
- Bouazza, G., Souabi, S., Madinzi, A., & Chatri, E. H. (2022). Optimization of the color corresponding to the different absorbencies of tannery wastewater by response surface designs. *WATER CONSERVATION & MANAGEMENT*, 6(2), 99–106. <https://doi.org/10.26480/wcm.02.2022.99.106>
- Brookshaw, D., Patrick, R., Lloyd, J., & Vaughan, D. (2012). Microbial effects on mineral-radionuclide interactions and radionuclide solid-phase capture processes. *Mineralogical Magazine*, 76(3), 777–806. <https://doi.org/10.1180/minmag.2012.076.3.25>
- Bullo, T. A., & Bayisa, Y. M. (2022). Optimizing the removal efficiency of chromium from tanning plant effluent by adsorption method with activated carbon chat stems (*Catha edulis*) using response surface methodology. *Water Conser Manag (WCM)*, 6(1), 15–21. <https://doi.org/10.26480/wcm.01.2022.15.21>
- d’Almeida, G., Kaki, C., & Adeoye, J. (2016). Benin and Western Nigeria Offshore Basins: A stratigraphic nomenclature comparison. *International Journal of Geosciences*, 7, 177–188. <https://doi.org/10.4236/ijg.2016.72014>
- Ding, D. X., Tan, X., Hu, N., Li, G. Y., Wang, Y. D., & Tan, Y. (2012). Removal and recovery of uranium (VI) from aqueous solutions by immobilized aspergillus niger powder beads. *Bioprocess and Biosystems Engineering*, 35(9), 1567–1576. <https://doi.org/10.1007/s00449-012-0747-8>
- Dong, Y., Yuan, H., Ge, D., & Zhu, N. (2022). A novel conditioning approach for amelioration of sludge dewaterability using activated carbon strengthening electrochemical oxidation and realized mechanism. *Water Research*, 220, 118704. <https://doi.org/10.1016/j.watres.2022.118704>
- Gan, Y., Wang, L., Yang, G., Dai, J., Wang, R., & Wang, W. (2017). Multiple factors impact the contents of heavy metals in vegetables in high natural background area of China. *Chemosphere*, 184, 1388–1395. <https://doi.org/10.1016/j.chemosphere.2017.06.072>
- Garba, N. N., Ramli, A. T., Saleh, M. A., Sanusi, S. M., & Gabdo, H. T. (2016). Radiological mapping of Kelantan, Malaysia, using terrestrial radiation dose rate. *Isotopes in Environmental and Health Studies*, 52(3), 214–218. <https://doi.org/10.1080/10256016.2016.1095189>
- Gautam, A. K., & Bhadauria, R. (2012). Characterization of aspergillus species associated with commercially stored triphala powder. *African Journal of Biotechnology*, 11 (104), 16814–16823. <https://doi.org/10.5897/AJB11.2311>
- Gerber, U., Zirnstein, I., Krawczyk-Bärsch, E., Lünsdorf, H., Arnold, T., & Merroun, M. L. (2016). Combined use of flow cytometry and microscopy to study the interactions between the gram-negative betaproteobacterium *Acidovorax facilis* and uranium (VI). *Journal of Hazardous Materials*, 317, 127–134. <https://doi.org/10.1016/j.jhazmat.2016.05.062>
- ICRP. (1991). Recommendations of the International Commission on radiological protection 1990 (ICRP) publication no. 60. *Annals of the ICRP*, 21, 1–201. <https://www.icrp.org/publication.asp?id=ICRP%20Publication%2060>
- International Atomic Energy Agency (IAEA). (1989). Measurement of radiation in food and the Environment; a guidebook. International Atomic Energy Agency (IAEA) Technical report series, 1989 No. 295.
- International Atomic Energy Agency (IAEA). (1996). *Radiation protection and the safety of radiation sources*. IAEA.
- International Commission on Radiological Protection (ICRP). (2012). *Compendium of dose coefficients based on ICRP publication 60 Annals of the ICRP* (p. 41). ICRP.
- Ire, F., & Ahuekwe, E. F. (2016). Production of fungal laccase using orange peelings as substrate by submerged static fermentation. *British Microbiology Research Journal*, 15(5), 1–19. <https://doi.org/10.9734/BMRJ/2016/27257>
- Isinkaye, M. O., & Emelue, H. U. (2015). Natural radioactivity measurements and evaluation of radiological hazards in sediment of Oguta Lake, South East Nigeria. *Journal of Radiation Research and Applied Sciences*, 8(3), 459–469. <https://doi.org/10.1016/j.jrras.2015.05.001>
- Jibiri, N. N., Alausa, S. K., & Farai, I. P. (2009). Radiological hazard indices due to activity concentrations of natural radionuclides in farm soils from two high background radiation areas in Nigeria. *International Journal of Low Radiation*, 6(2), 79–95. <https://doi.org/10.1504/IJLR.2009.028529>
- Joel, E. S., Omeje, M., Olawole, O. C., Adeyemi, G. A., Akinpelu, A., Embong, Z., & Saeed, M. A. (2021). In-situ assessment of

- natural terrestrial-radioactivity from uranium-238(238U) thorium-232(232Th). And potassium-40 (40K) in coastal urban-environment and its possible health implications. *Scientific Reports*, 11(1), 17555. <https://doi.org/10.1038/s41598-021-96516-z>
- Law, G. T., Geissler, A., Lloyd, J. R., Livens, F. R., Boothman, C., Begg, J. D., Denecke, M. A., Rothe, J., Dardenne, K., Burke, I. T., Charnock, J.M., & Morris, K. (2010). Geomicrobiological redox cycling of the transuranic element neptunium. *Environmental Science & Technology*, 44(23), 8924–8929. <https://doi.org/10.1021/es101911v>
- Lazareva, E. V., Zhmodik, S. M., Melgunov, M. S., Petrova, I. V., & Bryanskaya, A. V. (2011). Redistribution of radionuclides between a microbial mat and a carbonate body at the Garga hot spring (Baikal Rift Zone). *Doklady Earth Sciences*, 439(2), 1131–1137. <https://doi.org/10.1134/S1028334X11080174>
- Lerebours, A., Gudkov, D., Nagorskaya, L., Kaglyan, A., Rizewski, V. (2018). Impact of environmental radiation on the health and reproductive status of fish from Chernobyl. *Environmental Science & Technology*, 52(16), 9442–9450. <https://doi.org/10.1021/acs.est.8b02378>
- Li, X., Ding, C., Liao, J., Lan, T., Li, F., Zhang, D., Yang, J., Yang, Y., Luo, S., Tang, J., & Liu, N. (2014). Biosorption of uranium on *Bacillus* sp. dwc-2: Preliminary investigation on mechanism. *Journal of Environmental Radioactivity*, 135, 6–12. <https://doi.org/10.1016/j.jenvrad.2014.03.017>
- Liu, W., Huang, F., Liao, Y., Zhang, J., Ren, G. (2008). Treatment of Cr(VI)-containing mg (OH) 2 nanowaste. *Angewandte Chemie*, 47(30), 5619–5622. <https://doi.org/10.1002/anie.200800172>
- Liu, J., Li, H., Harvey, J., Airey, G., Lin, S., Lee, S. L. J., & Yang, B. (2023). Study on leaching characteristics and biotoxicity of porous asphalt with biochar fillers. *Transportation Research, Part D: Transport & Environment*, 122, 103855. <https://doi.org/10.1016/j.trd.2023.103855>
- Lopez-Fernandez, M., Vilchez-Vargas, R., Jroundi, F., Boon, N., Pieper, D., & Merroun, M. L. (2018). Microbial community changes induced by uranyl nitrate in bentonite clay microcosms. *Applied Clay Science*, 160, 206–216. <https://doi.org/10.1016/j.clay.2017.12.034>
- Lütke, L., Moll, H., Bachvarova, V., Selenska-Pobell, S., & Bernhard, G. (2013). The U (VI) speciation influenced by a novel *paenibacillus* isolate from Mont terri opalinus clay. *Dalton Transactions*, 42(19), 6979–6988. <https://doi.org/10.1039/c3dt33032j>
- McDougald, D., Rice, S. A., Weichart, D., & Kjelleberg, S. (1998). Nonculturability: Adaptation or debilitation? *FEMS Microbiology Ecology*, 25(1), 1–9. <https://doi.org/10.1111/j.1574-6941.1998.tb00455.x>
- Møller, A. P., & Mousseau, T. A. (2013). The effects of natural variation in background radioactivity on humans, animals and other organisms. *Biological Reviews of the Cambridge Philosophical Society*, 88(1), 226–254. <https://doi.org/10.1111/j.1469-185X.2012.00249.x>
- Mutiu, A. A., Gbolahan, I., Oluwaseyi, A. O., Folashade, H. F., Adeyemi, Y. A., Taofeeq, A. A., & Adelowo, A. A. (2013). Water quality assessment of Iju River in Ogun State, Nigeria: Effect of human activities. *Journal of Environmental Science, Toxicology and Food Technology*, 6(3), 64–68.
- Nazina, T. N., Luk'yanova, E. A., Zakharova, E. V., Konstantinova, L. I., Kalmykov, S. N., Poltarau, A. B., & Zubkov, A. A. (2010). Microorganisms in a disposal site for liquid radioactive wastes and their influence on radionuclides. *Geomicrobiology Journal*, 27(5), 473–486. <https://doi.org/10.1080/01490451003719044>
- Nazir, R., Khan, M., Masab, M., Rehman, H. U., Rauf, N. U. (2015). Accumulation of heavy metals (ni, Cu, cd, cr, pb, zn, fe) in the soil, water and plants and analysis of physico-chemical parameters of soil and water collected from Tanda Dam Kohat. *Journal of Pharmaceutical Sciences and Research*, 7(3), 89.
- Newsome, L., Morris, K., & Lloyd, J. R. (2014). The biogeochemistry and bioremediation of uranium and other priority radionuclides. *Chemical Geology*, 363, 164–184. <https://doi.org/10.1016/j.chemgeo.2013.10.034>
- Nguyen, X. P., Nguyen, D. T., Pham, V. V., & Bui, V. D. (2021). Evaluation of the synergistic effect in wastewater treatment from ships by the advanced combination system. *WATER CONSERVATION & MANAGEMENT*, 5(1), 60–65. <https://doi.org/10.26480/wcm.01.2021.60.65>
- Normality Testing, Skewness and Kurtosis. (2019). <https://help.gooddata.com/doc/en/reporting-and-dashboards/maql-analytical-query-language/maql-expression-reference/aggregation-functions/statistical-functions/predictive-statistical-use-cases/normality-testing-skewness-and-kurtosis>. (Retrieved February 15th, 2020).
- Nyarko, E., Botwe, B., Ansong, J., Delfanti, R., Barsanti, M., Schirone, A., & Delbono, I. (2011). Determination of 210Pb, 226Ra and 137Cs in beach sands along the coastline of Ghana. *Afr J Environ Pollut Health*, 9(2), 17–23.
- Omeje, M., Adewoyin, O. O., Joel, E. S., Ehi-Eromosele, C. O., Emenike, C. P. (2018). Natural radioactivity concentrations of 226Ra, 232Th, and 40K in commercial building materials and their lifetime cancer risk assessment in dwellers. *Human and Ecological Risk Assessment: An International Journal*, 24(8), 2036–2053. <https://doi.org/10.1080/10807039.2018.1438171>
- Omeje, M., Adewoyin Olusegun, O., Joel, E. S., Ikechukwu, B. I., Timothy-Terhile Mary, A., Okoro Emeka, E., & Saeed, M. A. (2021). Measurements of seasonal variations of radioactivity distributions in riverine soil sediment of ado-odo ota, south- West Nigeria: Probabilistic approach using Monte Carlo. *Radiation Protection Dosimetry*, 193(2), 76–89. <https://doi.org/10.1093/rpd/ncab027>
- Omeje, M., Ijeh, I., Oluwasegun, A., Ogunrinola, I., & Saeed, M. A. (2020). Spatial distribution of gamma radiation dose rates from natural radionuclides and its radiological hazards in sediments along river Iju, Ogun state Nigeria. *MethodsX*, 7, 101086. <https://doi.org/10.1016/j.mex.2020.101086>
- Orosun, M. M., Ajibola, T. B., Farayade, B. R., Akinyose, F. C., Salawu, N. B. (2021). Radiological impact of mining: New insight from cancer risk assessment of radon in water from Ifelodun beryllium mining, North-Central Nigeria using Monte Carlo simulation. *Arabian Journal of Geosciences*, 14, 1–9. <https://doi.org/10.1007/s12517-021-08670-3>
- Orosun, M. M., Usikal, M. R., & Oyewumi, K. J. (2020). Radiological hazards assessment of laterite mining field in Ilorin, north-central Nigeria. *International Journal of Radiation Research*, 18(4), 895–906. <https://doi.org/10.52547/ijrr.18.4.895>
- Orosun, M. M., Usikal, M. R., Oyewumi, K. J., & Achuka, J. A. (2020). Radioactivity levels and transfer factor for granite mining field in Asa, north-central Nigeria. *Heliyon*, 6(6), e04240. <https://doi.org/10.1016/j.heliyon.2020.e04240>
- Orosun, M. M., Usikal, M. R., Oyewumi, K. J., & Adagunodo, T. A. (2019). Natural radionuclides and radiological risk assessment of granite mining field in Asa, North-central Nigeria. *MethodsX*, 6, 2504–2514. <https://doi.org/10.1016/j.mex.2019.10.032>
- Orosun, M. M., Usikal, M. R., Oyewumi, K. J., Onumojor, C. A., Ajibola, T. B., Valipour, M., & Tibbett, M. (2022).

- Environmental risks assessment of kaolin mines and their brick products using Monte Carlo simulations. *Earth Systems and Environment*, 6(1), 1–18. <https://doi.org/10.1007/s41748-021-00266-x>
- Osuagwu, E. S., Olaifa, E., & Ottersen, G. (2018). Effects of oil spills on fish production in the Niger Delta. *PLoS One*, 13(10), e0205114. <https://doi.org/10.1371/journal.pone.0205114>
- Othman, F., ME, A. E., & Mohamed, I. (2012). Trend analysis of a tropical urban river water quality in Malaysia. *Journal of Environmental Monitoring*, 14(12), 3164–3173. <https://doi.org/10.1039/c2em30676j>
- Petit, P. C., Pible, O., Eesbeeck, V. V., Alban, C., Steinmetz, G. (2020). Direct meta-analyses reveal unexpected microbial life in the highly radioactive water of an operating nuclear reactor core. *Microorganisms [Internet]*, 8(12), 1857. <https://doi.org/10.3390/microorganisms8121857>
- Plymale, A. E., Wells, J. R., Pearce, C. I., Brislawn, C. J., Graham, E. B. (2021). Niche partitioning of microbial communities at an ancient vitrified hillfort: Implications for vitrified radioactive waste disposal. *Geomicrobiology Journal*, 38(1), 36–56. <https://doi.org/10.1080/01490451.2020.1807658>
- Rivasseau, C., Farhi, E., Compagnon, E., de Gouvion Saint Cyr, D., van Lis, R. (2016). *Coccomyxa actinabiotis* sp. nov. (Trebouxiophyceae, Chlorophyta), a new green microalga living in the spent fuel cooling pool of a nuclear reactor. *Journal of Phycology*, 52(5), 689–703. <https://doi.org/10.1111/jpy.12442>
- Roh, C., Kang, C., & Lloyd, J. R. (2015). Microbial bioremediation processes for radioactive waste. *Korean Journal of Chemical Engineering*, 32(9), 1720–1726. <https://doi.org/10.1007/s11814-015-0128-5>
- Sakthivadivel, M., Nirmala, A., Sakthivadivel, J., Mukhilan, R. R., & Tennyson, S. (2020). Physicochemical and biological parameters of water at industrial sites of metropolitan city of Chennai, Tamil Nadu, India. *WATER CONSERVATION & MANAGEMENT*, 4(2), 90–98. <https://doi.org/10.26480/wcm.02.2020.90.98>
- Salome, K. R., Green, S. J., Beazley, M. J., Webb, S. M., Kostka, J. E., & Taillefert, M. (2013). The role of anaerobic respiration in the immobilization of uranium through biomineralization of phosphate minerals. *Geochimica et Cosmochimica Acta*, 106, 344–363. <https://doi.org/10.1016/j.gca.2012.12.037>
- Sarro, M. I., Garcia, A. M., & Moreno, D. A. (2005). Biofilm formation in spent nuclear fuel pools and bioremediation of radioactive water. *International Microbiology*, 8(3), 223–230.
- Sattar, A. A. (2021). Preparation of novel hybrid (almond shell and pleurotus sajor caju) biosorbent for the removal of heavy metals (nickel and lead) from wastewater. *WATER CONSERVATION & MANAGEMENT*, 5(1), 1–7. <https://doi.org/10.26480/wcm.01.2021.01.07>
- Savvaidis, I., Kegos, T., Papagiannis, C., Voidarou, C., Tsiotsias, A. (2001). Bacterial indicators and metal ions in high mountain lake waters. *Microbial Ecology in Health and Disease*, 13(3), 147–152. <https://doi.org/10.3402/mehd.v13i3.8017>
- Shen, Y., Sun, P., Ye, L., & Xu, D. (2023). Progress of anaerobic membrane bioreactor in municipal wastewater treatment. *Science of Advanced Materials*, 15(10), 1277–1298. <https://doi.org/10.1166/sam.2023.4531>
- Singh, P. K., & Saxena, S. (2018). Towards developing a river health index. *Ecological Indicators*, 85, 999–1011. <https://doi.org/10.1016/j.ecolind.2017.11.059>
- Sousa, T., Chung, A. P., Pereira, A., Piedade, A. P., & Morais, P. V. (2013). Aerobic uranium immobilization by *Rhodanobacter* A2-61 through formation of intracellular uranium–phosphate complexes. *Metallomics*, 5(4), 390–397. <https://doi.org/10.1039/c3mt00052d>
- Stokell, J. R., & Steck, T. R. (2012). Viable but Nonculturable Bacteria. In L. S., Chichester (Ed.), *Encyclopedia of life sciences*. JohnWiley & sons. Ltd. <https://doi.org/10.1002/9780470015902.a0000>
- Stroes-Gascoyne, S., Hamon, C. J., & Maak, P. (2011). Limits to the use of highly compacted bentonite as a deterrent for microbiologically influenced corrosion in a nuclear fuel waste repository. *Physics and Chemistry of the Earth*, 36(17–18), 1630–1638. <https://doi.org/10.1016/j.pce.2011.07.085>
- Sudhakar, S., Moondra, N., & Christian, R. A. (2022). A comparative study on treatment of CETP wastewater using SBR and SBR-IFAS process. *WATER CONSERVATION & MANAGEMENT*, 6(1), 51–54. <https://doi.org/10.26480/wcm.01.2022.51.54>
- Tang, J., Zhang, J., Ren, L., Zhou, Y., Gao, J. (2019). Diagnosis of soil contamination using microbiological indices: A review on heavy metal pollution. *Journal of Environmental Management*, 242, 121–130. <https://doi.org/10.1016/j.jenvman.2019.04.061>
- Tang, T., Zhou, M., Lv, J., Cheng, H., Wang, H., Qin, D., & Liu, X. (2022). Sensitive and selective electrochemical determination of uric acid in urine based on ultrasmall iron oxide nanoparticles decorated urchin-like nitrogen-doped carbon. *Colloids and Surfaces B, Biointerfaces*, 216, 112538. <https://doi.org/10.1016/j.colsurfb.2022.112538>
- Tu, H., Lan, T., Yuan, G., Zhao, C., Liu, J. (2019). The influence of humic substances on uranium biomineralization induced by *Bacillus* sp. dwc-2. *Journal of Environmental Radioactivity*, 197, 23–29. <https://doi.org/10.1016/j.jenvrad.2018.11.010>
- Tuttle, M. L. W., Charpentier, R. R., & Brownfield, M. E. (1999). Tertiary Niger Delta (Akata- Agbada) Petroleum System (No. 719201), Niger Delta Province, Nigeria, Cameroon, and Equatorial Guinea, Africa. U.S. GEOLOGICAL SURVEY Open-file report 99-50-H (1999). <https://pubs.usgs.gov/of/1999/ofr-99-0050/OF99-50H/ChapterA.html>. (Retrieved September 20, 2021).
- Uluturhan, E., Kontas, A., & Can, E. (2011). Sediment concentrations of heavy metals in the homa lagoon (Eastern Aegean Sea): Assessment of contamination and ecological risks. *Marine Pollution Bulletin*, 62(9), 1989–1997. <https://doi.org/10.1016/j.marpolbul.2011.06.019>
- UNSCEAR. (2000). sources and effects of ionizing radiation. United Nations Scientific Committee on the Effects of Atomic Radiation. *Journal of Radiological Protection*, 21(1), 83–86. <https://doi.org/10.1088/0952-4746/21/1/60>
- VANGUARD. (2014). *FG crashes fish prices to affordable levels*. Vanguard news. <http://www.vanguardngr.com/2014/12/gf-crashes-fish-prices-affordable-levels/>
- Wang, Y. L., Wang, Q., Yuan, R., Sheng, X. F., & He, L. Y. (2019). Isolation and characterization of mineral-dissolving bacteria from different levels of altered mica schist surfaces and the adjacent soil. *World Journal of Microbiology and Biotechnology*, 35(1), 1–13. <https://doi.org/10.1007/s11274-018-2573-x>
- Wang, L., Zhang, J., Li, H., Yang, H., Peng, C., Peng, Z., & Lu, L. (2018). Shift in the microbial community composition of surface water and sediment along an urban river. *Science of the Total Environment*, 627, 600–612. <https://doi.org/10.1016/j.scitotenv.2018.01.203>
- Wu, H., Li, Y., Zhang, W., Wang, C., Wang, P. (2019). Bacterial community composition and function shift with the aggravation of water quality in a heavily polluted river. *Journal of*

- Environmental Management*, 237, 433–441. <https://doi.org/10.1016/j.jenvman.2019.02.101>
- Xiong, L., Bai, X., Zhao, C., Li, Y., Tan, Q., Luo, G., & Song, F. (2022). High-resolution data sets for global carbonate and silicate rock weathering carbon sinks and their change trends. *Earth's Future*, 10(8). <https://doi.org/10.1029/2022EF002746>
- Yin, L., Wang, L., Li, J., Lu, S., Tian, J., Yin, Z., & Zheng, W. (2023). YOLOV4\_CSPBi: Enhanced Land Target Detection Model. *Land*, 12(9), 1813. <https://doi.org/10.3390/land12091813>
- Yin, L., Wang, L., Li, T., Lu, S., Tian, J., Yin, Z., & Zheng, W. (2023). U-Net-LSTM: Time series-enhanced lake boundary prediction Model. *Land*, 12(10), 1859. <https://doi.org/10.3390/land12101859>
- Yin, L., Wang, L., Li, T., Lu, S., Yin, Z. (2023). U-Net-STN: A novel end-to-end lake boundary prediction model. *Land*, 12(8), 1602. <https://doi.org/10.3390/land12081602>
- Yuan, J., Li, Y., Shan, Y., Tong, H., & Zhao, J. (2023). Effect of magnesium ions on the mechanical properties of soil reinforced by microbially induced carbonate precipitation. *Journal of Materials in Civil Engineering*, 35(11), 4023413. <https://doi.org/10.1061/JMCEE7.MTENG-15080>
- Yu, Z., Xu, X., Guo, L., Jin, R., & Lu, Y. (2024). Uptake and transport of micro/nanoplastics in terrestrial plants: Detection, mechanisms, and influencing factors. *Science of the Total Environment*, 907, 168155. <https://doi.org/10.1016/j.scitotenv.2023.168155>
- Zhang, G., Zhao, Z., Yin, X., & Zhu, Y. (2021). Impacts of biochars on bacterial community shifts and biodegradation of antibiotics in an agricultural soil during short-term incubation. *Science of the Total Environment*, 771, 144751. <https://doi.org/10.1016/j.scitotenv.2020.144751>
- Zhang, G., Zhao, Z., & Zhu, Y. (2020). Changes in abiotic dissipation rates and bound fractions of antibiotics in biochar-amended soil. *Journal of Cleaner Production*, 256, 120314. <https://doi.org/10.1016/j.jclepro.2020.120314>
- Zhao, Y., Dong, Y., Chen, X., Wang, Z., Cui, Z., & Ni, S. (2023). Using sulfide as nitrite oxidizing bacteria inhibitor for the successful coupling of partial nitrification-anammox and sulfur autotrophic denitrification in one reactor. *Chem Eng J*, 475, 146286. <https://doi.org/10.1016/j.cej.2023.146286>
- Zhao, C., Li, X., Ding, C., Liao, J., Du, L. (2016). Characterization of uranium bioaccumulation on a fungal isolate *Geotrichum sp. dwc-1* as investigated by FTIR, TEM and XPS. *Journal of Radioanalytical and Nuclear Chemistry*, 310, 165–175. <https://doi.org/10.1007/s10967-016-4797-2>
- Zhou, G., Lin, G., Liu, Z., Zhou, X., Li, W., Li, X., & Deng, R. (2023). An optical system for suppression of laser echo energy from the water surface on single-band bathymetric LiDAR. *Optics and Lasers in Engineering*, 163, 107468. <https://doi.org/10.1016/j.optlaseng.2022.107468>